Ice-nucleating particle concentration measurements from Ny-Ålesund during the Arctic Spring-Summer in 2018

Matteo Rinaldi[1], Naruki Hiranuma[2], Gianni Santachiara[1], Mauro Mazzola[3], Karam Mansour[1,4,5], Marco Paglione[1], Cheyanne A. Rodriguez[2], Rita Traversi[6], Silvia Becagli[6], David Cappelletti[7,3], Franco Belosi[1]

[1]Institute of Atmospheric Sciences and Climate (ISAC), National Research Council (CNR), 40129 Bologna, Italy
[2]Department of Life, Earth and Environmental Sciences, West Texas A&M University, Canyon, TX, USA
[3]Institute of Polar Sciences (ISP), National Research Council (CNR), 40129 Bologna, Italy
[4]Department of Physics and Astronomy, University of Bologna, 40127 Bologna, Italy
[5]Department of Oceanography, Faculty of Science, University of Alexandria, 21511 Alexandria, Egypt
[6]Department of Chemistry "Ugo Schiff", University of Florence, 50019 Florence, Italy
[7]Dipartimento di Chimica, Biologia e Biotecnologie, Università degli Studi di Perugia, 06123 Perugia, Italy

Correspondence to: Matteo Rinaldi (m.rinaldi@isac.cnr.it)

Abstract.

In this study, we present atmospheric ice-nucleating particle (INP) concentrations from the Gruvebadet (GVB) observatory in Ny-Ålesund (Svalbard) in 2018. The ambient INP concentrations (*n*INP) were measured for aerosol particles collected on filter samples by means of two offline instruments: the Dynamic Filter Processing Chamber (DFPC) and the West Texas Cryogenic Refrigerator Applied to Freezing Test system (WT-CRAFT) to assess condensation and immersion freezing, respectively. DFPC measured *n*INPs for a set of filters collected through two size-segregated inlets: one for transmitting particulate matter less than 1 µm (PM_1) and another for that of less than 10 µm aerodynamic diameter (PM_{10}). Overall, $nINP_{PM10}$ measured by DFPC ranged from 3 to 185 m^{-3} at temperatures (*T*s) of -15 to -22°C. On average, the super-micrometer INP ($nINP_{PM10}$ - $nINP_{PM1}$) accounted for approximately 20-30% of $nINP_{PM10}$ in spring and increased markedly in summer. In particular, it contributed 45% at *T* of -22°C and 65% at *T* of -15°C. This increase trend of super-micron INP fraction towards summer suggests an important role of super-micrometer aerosol particles as the source of Arctic INPs. At the same *T* range, WT-CRAFT measured 1 to 199 m^{-3}. While the measured *n*INPs generally agree between these two datasets, a notable offset was observed in part because these two techniques assess different ice nucleation modes. We considered many factors possibly explaining the observed difference of our trustful techniques, and we conclude that a different sensitivity of Arctic INPs to different ice nucleation modes explains the observed discrepancy. Besides, our analysis of *n*INP and activated fraction (AF), INP scaled to the total aerosol particle concentration, revealed several important indications regarding the INP seasonal variability at GVB in 2018. Contrary to recent works (e.g., INP measurements from GVB in 2012), our results do not show a sharp increase of *n*INP from spring to summer. An increasing trend was observed for a subset of our data, but the spring-to-summer *n*INP enhancement ratios never exceeded a factor of three. A more evident spring to summer increase was found in our AF data, suggesting higher freezing efficiency of large aerosol particles at GVB in summer. Analysis of low-travelling

back-trajectories and meteorological conditions at GVB alongside our INP data suggests that the summer time INP population is influenced both by terrestrial (snow-free land) and marine sources. Our spatiotemporal analyses of satellite retrieved Chlorophyll-a as well as spatial source attribution indicates the maritime INPs are expected at GVB from the seawaters surrounding the Svalbard archipelago and/or in the proximity of Greenland and Iceland.

1 Introduction

The Arctic is a climate-change sensitive region and is experiencing a higher temperature (*T*) increase, as compared to mid latitudes, due to the phenomenon called Arctic amplification (Serreze and Barry, 2011). While sea ice-albedo feedback appears to be a clear factor, the roles of other processes are difficult to quantify. Especially, contributions from forcing and feedback mechanisms associated with aerosol particles that can trigger heterogeneous ice nucleation and Arctic mixed-phase cloud formation remain uncertain and unpredictable (Murray et al., 2021).

The Arctic mixed-phase clouds are composed of both ice and supercooled liquid water and structured in persistent stratiform layers (Shupe et al., 2006; Shupe et al., 2011). In mixed-phase clouds, the phase of hydrometeors formed through aerosol-cloud interactions plays an important role in determining cloud albedo and lifetime (de Boer et al., 2014). A strong sensitivity of stratiform mixed-phase cloud lifetime to the number of ice crystals was reported by Harrington and Olsson (2001) and Jiang et al. (2000). This effect was attributed in part to the Wegener-Bergeron-Findeisen mechanism (Bergeron, 1935; Findeisen, 1938; Wegener, 1911), for which ice grows at the expense of liquid water due to its lower saturation vapor pressure. The resulting microphysical instability can glaciate clouds within a few hours or less (Jiang et al., 2000; Pinto, 1998; Rangno and Hobbs, 2001; Harrington et al., 1999). Thus, the presence of aerosol particles that can trigger heterogeneous ice nucleation (ice-nucleating particles, INPs, hereafter) in the Arctic atmosphere can potentially have substantial impacts on precipitation formation, cloud radiative properties and climate (Solomon et al., 2018; Murray et al., 2021).

Atmospheric heterogeneous ice nucleation occurs through four different major pathways: deposition, condensation, immersion and contact freezing (Pruppacher and Klett, 2010; Vali et al., 2015). Ice formation by deposition occurs when the ambient is supersaturated with respect to ice but under water-subsaturated condition, and ice forms through water vapour deposition on INP. In condensation freezing, ice forms as water vapor condenses on a condensation nucleus at subzero *T*s, while a nucleus immersed in a supercooled water droplet freezes in immersion freezing. In contact freezing, an extramural INP promotes freezing when it contacts with a supercooled droplet. The distinction between condensation-freezing and immersion-freezing is still matter of debate (Dymarska et al., 2006). Nevertheless, the recent results of Wex et al. (2014) and Hiranuma et al. (2015) suggest that they might be the same process. In general, INPs can be of abiotic (e.g., mineral dust, volcanic ashes and soil dust) or biotic (e.g., bacteria, fungi, microalgae and pollen) origin (Hoose and Mohler, 2012; Murray et al., 2012). Sea water has been identified to be a source of ice active organic matters (Knopf et al., 2011; Wang et al., 2015; Wilson et al., 2015), which are transferable to the atmosphere within sea spray particles (e.g., McCluskey et al., 2017). Mineral particles are dominant immersion and condensation mode INPs typically below -20°C according to Fig. 13 in Hoose and Mohler (2012),

with an exception of K-feldspar, which facilitates ice nucleation at much higher *T*s when compared to other mineral compositions (Atkinson et al., 2013). Further, biogenic INPs tend to support formation of ice at *T*s relatively higher than abiotic INPs (Murray et al., 2012), even though there is a considerable variation in ice nucleation efficiency within biotic INPs (Kanji et al., 2017).

Only a few multi-season measurements of Arctic INP concentration (*n*INP) are currently available. A summary of previous ground-based *n*INP measurements and reported *T* ranges can be found in Table 1. The first ground level *n*INP data from the Arctic region are those by Borys (1983). Measurements were performed with an offline dynamic condensation chamber at *T* between -28 and -16°C in water saturation condition. It was observed that pollution from lower latitudes did not act as efficient INPs and, thereby, contributed insignificantly to the Arctic atmosphere as low *n*INP values coincided with the Arctic haze period. Next, Bigg (1996) measured INPs active at -15°C in a static chamber and at humidity just above 100%, during an icebreaker cruise to the North Pole. The Ocean was considered to be a prevalent source of INPs, based on the high negative correlation between *n*INP and the time since the sampled air masses have been over the open ocean. Similar measurements were performed by Bigg and Leck (2001) in the central Arctic ocean (20 July – 18 September 1996). The authors identified bacteria and probable submicron fragments of marine organisms in the samples and suggested to be the source of INPs in the Arctic.

More recent measurements were mostly performed in the immersion freezing mode. Conen et al. (2016) measured *n*INP at a coastal mountain observatory in Northern Norway. During the summer, the authors observed that *n*INP (*T* of -15°C) in oceanic air tripled after about one day of passage over land. Both marine and terrestrial INP sources were identified by Creamean et al. (2018) in the Northern Alaskan Arctic during spring. Irish et al. (2019) measured *n*INP in the Canadian Arctic marine boundary layer during summer 2014 on board the research ship Amudsen. The *n*INP values were positively correlated with the total residence time over land and negatively correlated with the total residence time over sea ice and open water, suggesting higher contribution of mineral dust particles than sea-spray related sources. Similar conclusions were found by Si et al. (2018) from measurements performed in the Canadian Arctic. Mason et al. (2016) found that a large fraction of the observed INPs belonged to the coarse size range, through spring and summer seasons at Alert station. Likewise, a size dependent ice nucleation efficiency, with larger particles being more ice active, was reported by Creamean et al. (2018) and Si et al. (2018). Recently, some studies reported a marked *n*INP seasonal variability in the Atlantic sector of the Arctic (Wex et al., 2019; Tobo et al., 2019; Santl-Temkiv et al., 2019). In particular, Wex et al. (2019) observed an increase of *n*INP of more than one order of magnitude from spring to summer (e.g., ~14 times at T=-15°C) at GVB in 2012. Tobo et al. (2019) focused on two field campaigns held at Mt. Zeppelin, in July 2016 (six samples) and March 2017 (seven samples). They report *n*INPs at -20°C of about 0.01 L^{-1} in spring and about 0.1 L^{-1} in summer. This increase was interpreted as the effect of local INP sources active when land and sea are free from snow and ice (Santl-Temkiv et al., 2019; Wex et al., 2019). Conversely, Schrod et al. (2020) presented the results of multi-year (May 2015 - January 2017) INP observations at Mt. Zeppelin (Svalbard), evidencing no significant seasonal trend in *n*INP.

In the present study, we contribute to fill the present gap of INP observations in the Arctic environment, investigating *n*INP and potential sources at the ground level site of GVB (Svalbard), through spring and summer time measurements, by two INP quantification techniques, representing immersion and condensation freezing. We hypothesized that the *n*INP variability at a single *T* can be explained by differences in freezing modes. Recent modeling simulation and remote sensing studies suggest immersion freezing is the most relevant heterogeneous ice nucleation mechanism in mixed-phase clouds, which are prevalent in the Arctic (Hande and Hoose, 2017; Westbrook and Illingworth, 2011). The key to verify this in the Atlantic sector of the Arctic depends on a multitude of ambient INP measurements with a combination of trustful INP measuring systems at wide heterogeneous ice-nucleating conditions. Finally, we investigate the ice nucleation efficiency of Arctic aerosol particles represented by the activated fraction (AF), which provides further insight into the seasonal trend of ice nucleation efficiency besides concentration data.

2 Methods

2.1 Sampling

The aerosol particle sampling was performed at the GVB observatory, located in proximity of the village of Ny-Ålesund (78°55' N, 11°56' E) on the Spitsbergen Island, Svalbard (Fig. 1). The observatory is about 40 m above sea level, located about 1 km south-west of the village. This position guarantees minimal influence by local sources of pollution as the South wind prevails (Udisti et al., 2016). Aerosol particle sampling activities for offline *n*INP analyses were arranged independently for the two methods (see Sect. 2.2) with different sampling time intervals through different inlets. Nevertheless, the inlets were all located at the same altitude, about 5 m above the ground level.

For the Dynamic Filter Processing Chamber (DFPC) application, aerosol particle samples were collected on nitrocellulose membrane filters (Millipore HABG04700, nominal porosity 0.45 µm). We deployed two parallel sampling inlet systems, one with a PM_1 size-cut and the other for PM_{10} (cut-point-Standard EN 12341, TCR Tecora). The operative flow was 38.3 (±2.0) lpm in each sampling line and was generated by two independent pumps (Bravo H Plus, TCR Tecora). The sampling activity for DFPC occurred over two meteorological seasons: between 17 April and 2 May 2018 in spring and between 11 and 27 July 2018 in Summer. A pair of samples through two inlet systems was collected each day, with a sampling duration of 3 to 4 hours. Our short sampling span was employed to avoid any aerosol particle overloading on filters. The sampling generally started in the morning during the spring campaign, while it started typically in the afternoon during the summer campaign (in coordination with other scheduled activities at GVB). Samples were stored at room *T* until analysis.

For the application of West Texas Cryogenic Refrigerator Applied to Freezing Test system (WT-CRAFT) analysis, a total of 28 samples were collected from April 16 to August 15, 2018. Aerosol particles were collected using 47 mm membrane filters (Whatman, Track-Etched Membranes, 0.2 µm pore). Briefly, aerosol particle-laden air was drawn from a central total suspended particulate (TSP) inlet with a constant average inlet flow of 5.4 lpm (± 0.2 lpm standard deviation). We note that the TSP inlet is custom made, and is designed to operate with isokinetic and laminar flow at 150 lpm. From the central inlet,

an 8 mm outside diameter stainless steel tube was directly connected to the filter sampler to intake a subset of air flow. More detailed conditions of our filter sampling, including sampling time stamps, air volume sampled through filter cross section, and the resulting HPLC water volume used to suspend aerosol particles for WT-CRAFT analysis, are summarized in Table S1. Below the filter sampler, the filtered-air was constantly pumped through a diaphragm pump (KnF, IP20-T). A critical orifice was installed upstream of the pump to ensure a constant volume flow rate and control the mass flow rate through the sampling line. A typical sampling interval was approximately 4 days with only one exception (i.e., 8 days for the sample collected starting on 26 May 2018).

2.2 Ice Nucleation Measurements

2.2.1 DFPC

All DFPC measurements were carried out in the lab, after completion of the campaigns, by the membrane filter technique following the procedure presented in Santachiara et al. (2010) and Rinaldi et al. (2017). All analysis was completed within ca. 6 months from sampling. A replica of the Langer dynamic filter processing chamber housed in a refrigerator was used to determine *n*INP at different *T*s. Before the analysis, each filter was placed on a metal plate (5.5 cm diameter, 0.5 mm thick), pre-covered with a smooth surface of paraffin, to ascertain good thermal contact of the filter with the supporting substrate. Subsequently, the paraffin was flash heated at 70°C for less than 5 seconds and rapidly cooled in order to fill the filter pores. By controlling the *T*s of the filter and of the surrounding air, saturated after contact with finely minced ice, it was possible to expose the samples to different *T*s by keeping the water saturation ratio (S_w) above 1. The supersaturation ratio was calculated theoretically from vapour pressures of ice and water at the considered *T*s (Buck, 1981).
The ice nucleation was visually evaluated by counting the number of ice crystal growing on individual aerosol particles on the sampled filter, illuminated by a visible light source. Measurements were performed at activation *T*s of -15°C, −18°C and −22°C and at S_w = 1.02. Uncertainties for air *T,* filter *T* and S_w are about 0.2°C, 0.1°C and 0.02, respectively. The overall uncertainty in the DFPC-based INP assessment was estimated to be around ±30%, by considering the effect of S_w variations on *n*INP extrapolated from the laboratory results by Belosi et al. (2018). The filter background INP contribution was evaluated by analysing blank filters at the same conditions as we evaluated the samples. Measurements were corrected for the filter background.

2.2.2 WT-CRAFT

To complement the DFPC results, we also used an offline droplet-freezing assay instrument, WT-CRAFT, to measure *T*-resolved *n*INP at *T* > -25°C, with a detection capability of >1 INP per m^3 of air. All analyses were completed within one year from collection of the samples; the samples were stored in a fridge (4°C) before analysis. While WT-CRAFT is originally a replica of NIPR-CRAFT (Tobo, 2016), the two CRAFT systems possess different sensitivities to artifact and detectable *T* ranges as described in Hiranuma et al. (2019) and Vepuri et al. (2021). The reason of different detectable *T* ranges is not

known. As shown in Hiranuma et al. (2019, i.e., Table S2), the uncertainties of T, reported by a sensor manufacturer (TGK, SN-170N), as well as ice nucleation efficiency in WT-CRAFT are ± 0.5°C and ±23.5%, respectively. Note that our ice nucleation uncertainty was estimated based on the average standard deviation across the examined T (T > -25°C) for known composition (microcrystalline cellulose), which reasonably matches with 95% confidence intervals of individual measurements (i.e., Eq. 3.21 of Schiebel (2017)). While there are no major differences between two CRAFT instruments, WT-CRFAT employs different image recording systems, stage and clean housing as compared to NIPR-CRAFT. For imaging, WT-CRAFT uses a combination of an Opti-Tekscope OT-M HDMI microscope camera and a Logitech c270 camera. This combination is used to correctly capture the transition of droplet brightness/contrast to opaque ice with 30 frame per second time resolution with a reasonable pixel resolution as well as magnification (if needed). As for a cold stage, we use a thin (<5 mm) polished aluminium plate to warrant an efficient thermal cooling and to make sure the Cryo-cooler system T is equivalent to the T measured at the surface of the plate within known uncertainties. Finally, WT-CRAFT is operated in a vertical clean bench (LABCONCO, Purifier®). All droplet preparations (70 × 3µL) were conducted in the clean bench to minimize the chance of contamination from the lab air.

Next, we briefly explain our experimental procedure. For each experiment, 70 solution droplets (3 µL each) placed on a hydrophobic Vaseline layer were analyzed. With a cooling rate of 1°C min^{-1}, we manually counted cumulative number of frozen droplets based on the color contrast shift in the off-the-shelf video recording camera. Afterwards, nINP of 3µL-sized droplets containing aerosol particles from the samples were estimated as a function of T for every 0.5°C. Prior to each WT-CRAFT experiment, we suspended particles on an individual filter sample in a known volume of ultrapure water, High Performance Liquid Chromatography (HPLC) grade, in which the first frozen droplet corresponded to 1 INP m^{-3} (Table S1). More specifically, our suspension-generating protocol followed (1) cutting the filter in two and soaking one filter half in ultrapure water in a sterilized falcon tube, (2) vortex-mixing the suspension tube to scrub particles on the filter in suspension, (3) applying an idle time of 5 min to have the quasi-steady state suspension, and (4) preparation of droplets out of the suspension through micro-pipetting in the clean bench. If necessary, the suspension sample was diluted until we observe their freezing spectrum collapsed onto the water background curve. Our diluted spectra and original freezing spectrum reasonably agreed in their overlapped T region (within a factor of three at the most) without any notable artifacts at T above -25°C. Due to the absence of failure, we simply stitched all spectra in the way that the data point with better (smaller) 95% confidence interval represent $n_{INP}(T)$ for the overlapping T region if observed.

2.2.3 Derivation of INP atmospheric concentrations

For DFPC samples, nINP, expressed hereafter in units of m^{-3}, was calculated by dividing the number of ice crystals quantified on each filter by the sampled volume of air passed through the filter. For the WT-CRAFT analysis, we first computed the $C_{INP}(T)$ value, which is the nucleus concentration in HPLC suspension (L^{-1} water) at a given T as described in Vali (1971). This $C_{INP}(T)$ value was calculated as a function of unfrozen fraction, $f_{unfrozen}(T)$ (i.e., the ratio of number of droplets unfrozen to the total number of droplets) as:

$$C_{INP}(T) = -\frac{\ln(f_{\text{unfrozen}}(T))}{V_d} \quad (1)$$

in which, V_d is the volume of individual droplets (3 μL). Next, we converted $C_{INP}(T)$ to *n*INP(T). The cumulative *n*INP per unit volume of sample air, described in DeMott et al. (2017), was estimated as:

$$nINP(T) = C_{INP}(T) \times DF \times \frac{V_l}{V_{air}} \quad (2)$$

where DF is a serial dilution factor (e.g., DF = 1 or 10 or 100 and so on). The sampled air volume (V_{air}) and the suspension volume (V_l) are now provided in Table S1.

To estimate the efficiency of the sampled aerosol particles to nucleate ice, we calculated the INP Activated Fraction (AF), by scaling *n*INP to the aerosol particle number concentration measured onsite in parallel (see 2.3.1). For our AF estimation in this study, only aerosol particles in the 0.5-10 µm size range were considered, as this size range is reasonably accountable for heterogeneous ice nucleation in the atmosphere (Kanji et al., 2017).

2.3 Complementary Analyses

2.3.1 Particle size distribution measurements

The aerosol particle number size distribution was continuously monitored at the GVB station during all the sampling activities using a Scanning Mobility Particle Sizer (SMPS) model TSI 3034 for the diameter range between 10 and 500 nm (54 channels). An Aerodynamic Particle Sizer (APS) model TSI 3321 was used for measuring the aerodynamic aerosol particle diameters between 0.5 and 20 micrometers in the side-by-side position of SMPS. Both instruments are connected to a common multiple inlet, where the WT-CRAFT filter sampler was deployed, and record data averaged over 10 minutes (Giardi et al., 2016; Lupi et al., 2016). The aerodynamic diameters measured by the APS were corrected to the volume equivalent diameters using an average particle mass density equal to 1.95 g cm^{-3}, assuming a mixture of different substances based on the findings from Lisok et al. (2016), and a dynamic shape factor of 1. The number concentration in the resulting overlapping range was taken from the SMPS data as SMPS provides more size bins. At the end, commutative aerosol particle counts of SMPS and APS were considered as a total aerosol particle number concertation. To compare with *n*INP and to calculate the AF, the particle number concentrations at 10 minutes time resolution were averaged over each filter sampling period. The SMPS-APS measurements ran continuously during our aerosol particle sampling period except during the maintenance occurred in August, 2018.

2.3.2 Meteorology

Meteorological parameters (*T*; pressure, P; relative humidity, RH; wind speed, WS) were taken from those continuously provided by the Amundsen-Nobile Climate Change Tower, positioned less than 1 km N-E of GVB (Mazzola et al., 2016), while precipitation data (type and amount) from the eKlima database, provided by the Norwegian Meteorological Institute (https://seklima.met.no/observations/).

2.3.3 Offline Chemical Analysis

The chemical analysis of major and trace ion species, used in this work as aerosol particle source tracers, was accomplished on Teflon filters (PALL Gelman) collected at GVB by means of a TECORA Skypost sequential sampler equipped with a PM_{10} sampling head and an operating flow rate of 2.3 m^3 h^{-1} (EN 12341). The filters were handled with care (working under a class 100 laminar flow hood by personnel wearing powder free latex gloves to minimize potential contamination) throughout the sampling and offline analysis at the University of Florence. After sampling the filters were stored and shipped at -20°C. The measurements were carried out by a triple Dionex ThermoFisher Ion Chromatography system equipped with electrochemical-suppressed conductivity detectors. In particular, a Dionex AS4A-4 mm analytical column with a 1.8 mM Na_2CO_3/1.7 mM $NaHCO_3$ eluent, was used for the determination of most of inorganic anions (Cl^-, NO_3^-, SO_4^{-2}, $C_2O_4^{-2}$) while a Dionex AS11 separation column with a gradient elution (0.075–2.5 mM $Na_2B_4O_7$ eluent) was used for the measurement of F^- and some organic anions (acetate, glycolate, formate and methanesulfonate). Cationic species (Na^+, NH_4^+, K^+, Mg^{2+}, Ca^{2+}) have been determined by a Dionex CS12A-4 mm analytical column with 20 mM H_2SO_4 as eluent. Further analytical details can be found in Udisti et al. (2016) and Becagli et al. (2011).

2.3.4 Back trajectories and satellite ground type maps

In order to investigate the sources that contributed to INPs (i.e., maritime vs. terrestrial), we performed the 5-day back trajectory analysis, following Wex et al. (2019). For this analysis, 5-day back-trajectory air masses (HYSPLIT4 with GDAS data: https://ready.arl.noaa.gov/) from the National Oceanic and Atmospheric Administration (NOAA) HYSPLIT model (Rolph et al., 2017; Stein et al., 2015) were simulated for an altitude of 100 m above mean sea level (amsl) over the GVB station. For DFPC samples, the back-trajectories arrival time was considered simultaneous to INP samples, while for WT-CRAFT, the trajectories were calculated 2 times (06 and 18 UTC) a day covering the INP sampling period from April to August. Only back-trajectories travelling up to an altitude of 500 m amsl, were considered for this analysis, which is a reasonable assumption for air-masses passing within the marine boundary layer.

Ground condition maps were obtained from the National Ice Center's Interactive Multisensor Snow and Ice Mapping System (IMS) (Helfrich et al., 2007; National Ice-Center, 2008), National Snow & Ice Data center (NISDC; https://nsidc.org/). We used the daily Northern Hemisphere maps with a resolution of 4 km. The considered ground types were “seawater”, “sea-ice”," “land”, and “snow”. Seawater indicates passage of the air mass over open seawaters, while sea-ice indicates passage over ice-covered seawaters. Categories land and snow indicate passage of the air mass over land without and with snow cover, respectively. For each back-trajectory end-point, we applied nearest-neighbour interpolation in space and time to find the closest pixels on the satellite map and associated the end-point with the corresponding ground type. Combining the information obtained along the whole back-trajectory (or group of back-trajectories, for WT-CRAFT samples) it was possible to estimate the contribution of each ground type to each INP sample.

2.3.5 Satellite chlorophyll-a data and correlation analysis

Satellite retrieved chlorophyll-a fields were used to track the evolution of oceanic biological activity in the Arctic ocean during the study period. The best estimate "Cloud Free" (Level-4) daily sea surface chlorophyll-a concentration (CHL; mg m^{-3}) data were downloaded from the EU Copernicus Marine Environment Monitoring Service (CMEMS; http://marine.copernicus.eu/) based on a multi-sensor approach (i.e., SeaWiFS, MODIS-Aqua, MERIS, VIIRS and OLCI-S3A). The Level-4 product is available globally at ~4 km spatial and daily time resolution. From this global dataset, CHL fields were extracted in the Arctic Ocean during summer 2018 to be merged with INPs data.

Recent literature (Wilson et al., 2015; Knopf et al., 2011; Wang et al., 2015) has showed that sea-spray organics can nucleate ice being potentially important INPs in the clean marine atmosphere. Mansour et al. (2020b) evidenced that *n*INP over the North Atlantic Ocean follows the patterns of marine biological activity as traced by surface CHL concentration. The relationship between INPs and phytoplankton biomass, in terms of CHL concentration, was investigated excluding the samples clearly influenced by land inputs, to focus only on INPs potentially originated from the sea. The DFPC dataset was chosen to run this analysis because it provides a higher time-resolution than the WT-CRAFT one, and because it allows to differentiate between fine and coarse INPs. Each DFPC sample collected at a certain day has been considered as representative for that day, in order to be compared with the daily CHL time-series. The Pearson correlation coefficients between INPs and satellite-derived ocean color data, obtained by standard least squares regression, were computed at each grid point of the Arctic domain, and for different time-lags, to obtain the correlation maps presented in the results section.

2.3.6 Concentration weighted trajectory

The allocation of regional source areas potentially affecting *n*INPs sampled at GVB was achieved by applying the concentration weighted trajectory (CWT) model (Hsu et al., 2003; Jeong et al., 2011). In this procedure, each grid cell within the studied domain is associated to a weighted concentration, which is a measure of the source strength of a grid cell with respect to concentrations observed at the sampling site. The average weighted concentration in the grid cell (i, j) is determined by Eq. (3).

$$CWT_{ij} = \frac{\sum_{t=1}^{L} C_t D_{ijt}}{\sum_{t=1}^{L} D_{ijt}} \times W_{ij} \quad (3)$$

Where t is the index of the trajectory, L is the total number of trajectories (5 days – hourly time step), C_t is the INP concentration observed at sampling location (receptor site) on arrival of trajectory t, and D_{ijt} is the residence time (time spent) of trajectory t in the grid cell (i, j). Given C_t for INP, D_{ijt} can be determined by counting the number of hourly trajectory segment endpoints in each grid cell for each trajectory. This was repeated for all the back trajectories L. A high value for CWT_{ij} means that air parcels traveling over the grid cell (i, j) would be, on average, associated with elevated concentrations at the receptor site.

In this study, five-day low (< 500 m) air mass back-trajectories were used to produce the CWT spatial distribution corresponding to the DFPC summer campaign. The DFPC summer dataset was selected for consistency with the correlation analysis presented in the previous Section. Two trajectories per day were associated to the corresponding *n*INP of the day. Similar to the correlation analysis, the INP samples with a clear influence from land were excluded to consider only marine sources. The selected domain extends up to the limits of the area covered by the above-described low back-trajectories (48° – 85° N & 75° W – 42° E) and was divided into 1°×3° latitude/longitude grid cells (1443 cells, 308 cells with at least one trajectory endpoint). In order to reduce the impact of grid cells containing a low number of endpoints, for which the calculation of the CWT is statistically less robust, the CWT values were multiplied by a weighting factor (W_{ij}) according to Eq. (4).

$W_{ij} = 1$ (if $D_{ij} \geq median$), $W_{ij} = 0.8$ (if $3 < D_{ij} < median$), and $W_{ij} = 0$ (if $D_{ij} \leq 3$) (4)

The introducing of the weighing factor reduces the number of considered cells to 203.

3 Results

3.1 INP atmospheric concentration

Figure 2 shows the overall *n*INP range measured for aerosol particle samples from the GBV station in spring-summer 2018. While both measurements show reasonable agreement at -22°C in terms of *n*INP, a notable offset was observed between the two techniques. Specifically, *n*INP measured in condensation mode (DFPC) resulted generally higher than those measured in immersion mode (WT-CRAFT), and the deviation became even more apparent towards higher *T*. On average, $n\text{INP}_{\text{DFPC}}$ was 3 times higher than $n\text{INP}_{\text{WT-CRAFT}}$ at *T* = -22°C and 8 times higher at T= -15°C. Thus, the WT-CRAFT ice nucleation spectra presented a steeper ΔnINP/ΔT slope than the DFPC ones.

The DFPC-measured *n*INP values (PM_{10} size range) from GVB during the spring campaign ranged 55-185 (median 115), 5-90 (53) and 3-37 (20) m^{-3}, for *T* of -22, -18 and -15°C, respectively. During the summer campaign, the *n*INP ranges were 33-135 (median 77), 18-107 (45) and 6-66 (20) m^{-3}, for the same *T*s (Fig. 2). The WT-CRAFT analysis found no ice nucleation activity above -9°C in our GVB samples. Between -9 and -14°C a subset of the samples (<50%) presented *n*INP above the detection limit, with concentrations < 3 m^{-3}. In the rest of the *T* spectrum, *n*INP ranged 1-3 (median 2) m^{-3}, at *T* of -14°C and 24-9082 (166) m^{-3}, at *T* of -25°C.

A compilation of *n*INP values from previous ground level observations at various Arctic stations can be found in Table 1. The range of *n*INP from Table 1 is roughly comprised between 10^{-2} and 10^{3} m^{-3}, which encloses the majority of our measurements. We note that the comparison to these past studies is only qualitative given the great variability of parameters that could influence *n*INP (e.g., different instruments, locations, season, weather conditions, aerosol particle size distribution, ice nucleation mode, etc.). Regardless, both the DFPC and WT-CRAFT datasets fairly overlap with the *n*INP results reported in Wex et al. (2019), especially for *T*s below -15°C. The authors showed *n*INP previously measured at the same GVB station, during spring and summer 2012. The comparison between the *n*INP data from this study relative to Wex et al. (2019) can be

seen in Fig. 2. While this figure provides only a qualitative comparison as two studies examined different aerosol particles collected in different years, we found several interesting agreements and disagreements. First, at T = -22°C, Wex et al. (2019) report a very narrow concentration range (27-33 m^{-3}), resulting from only three samples, while DFPC and WT-CRAFT measurements span a much wider range (ca. 3-200 m^{-3}). The upper limit of observable *n*INP in Wex et al. (2019) was roughly 40 m^{-3}, depending on the volume of air sampled onto the analysed filters. On the contrary, the data ranges are in good agreement for *T*s over -18 to -15°C. Finally, the data from Wex et al. (2019) span over a wider range (ca. 10^{-1} – 10 m^{-3}) than WT-CRAFT ones (1-3 m^{-3}) for T> -15°C. The difference in the lower limit of the observations is due to different detection limits of WT-CRAFT (1 m^{-3}) and Wex et al. (2019) immersion freezing (ca. 10^{-1} m^{-3}) measurements.

Overall, the *n*INP range found in this study (e.g., ~1 to ~200 m^{-3} for T of -22°C) is quite substantial and indeed non-negligible in the Arctic. In different geographical locations and samples, our ice nucleation measurement techniques showed various ranges of *n*INPs. For example, Vepuri et al. (2021) showed that the average *n*INP in precipitation samples collected in West Texas (rural terrestrial environment) during 2018-2019 was approx. 480 m^{-3} at -15°C. Previous DFPC measurements in remote conditions at Mace Head (Ireland), during an intensive observation period in August 2015 (McCluskey et al., 2018b) showed *n*INP, in carefully selected clean marine air masses, in the range 0.4-15 and 2-40 m^{-3} for PM_1 and PM_{10} samples (T = -22°C), respectively, which is about one order of magnitude lower than what observed at GVB in 2018. If we compare with recent measurements performed at lower latitudes by DFPC, *n*INP over the Arctic was lower than those observed in continental European sites (San Pietro Capofiume, Po Valley, Italy; Belosi et al. (2017) and Rinaldi et al. (2017)), but comparable or even higher with respect to those observed at high altitudes (Monte Cimone, Norther Apennines, Italy; Rinaldi et al. (2017)) or at a Mediterranean coastal location (Capogranitola, Southern Sicily; Rinaldi et al. (2019)).

3.2 Contribution of fine and coarse INPs

The sampling strategy adopted for DFPC measurements allowed to investigate in fine (< 1 µm) and coarse (>1 µm) INPs. Table 2 reports the number concentrations of INPs measured in the two different size ranges, together with the average contribution of super-micrometer (coarse) INPs, derived by difference. In addition, scatterplots of $nINP_{PM10}$ vs $nINP_{PM1}$ are available in Fig. S1. A small contribution from coarse INPs characterized the spring campaign (~20%), suggesting that the dominant INP sources may be located at long distances (scale of the order of 100s-1000s km), with consequent depletion of the largest particles during transport, due to their higher gravitational deposition velocities. This result is consistent with previous works highlighting the contribution of long range transport from lower latitudes during the Arctic spring (Shaw, 1995; Heidam et al., 1999; Stohl, 2006). During the summer campaign, a significant ($p<0.005$) increase of the contribution of coarse INPs was observed (i.e., 65% at T = -15°C), resulting from the contribution of locally emitted aerosol particles (see Sect. 3.6) in part from the surface exposed to the air after snow and ice melting. While these coarse INP fraction estimation, presented in Table 2, involves substantial uncertainties, the same trend is inferred by the particle size distribution measurements, which show a significant ($p<0.01$) enhancement of coarse particles contribution in summer (median 30%) with respect to the spring time (median 16%) (Fig. S2). The increase of coarse INP contribution, from spring to summer time, is progressively more

pronounced with increasing activation *T*. A similar coarse fraction dominated INP population was reported by Mason et al. (2016) for measurements performed between 29 March to 23 July 2014 at the Alert Arctic station, with increasing coarse INPs contribution as a function of the activation *T*. Our results are unique compared to past studies as our measurements and data support the increase of coarse INP contribution during the meteorological season transition from spring to summer with increasing activation *T*.

3.3. Aerosol particle Activated Fraction (AF)

Figure 3 presents the aerosol particles AF as a function of *T* derived from the data of DFPC and WT-CRAFT. For DFPC, AF ranged from ~10^{-6} to 6×10^{-4} in its examined *T*s. Likewise, the AF range of WT-CRAFT was from 7×10^{-7} (minimum value observed at *T* of -10°C) to 6×10^{-4} (maximum value observed at *T* of -25°C). The seasonal evolution of the aerosol particles AF will be discussed in detail in the following Section (Sect. 3.4).

According to the size segregated DFPC data (Fig. 3a and b), generally higher ice nucleation efficiencies can be found in coarse particles when compared to sub-micrometer ones. This was particularly evident during the summer campaign, when the AF of coarse particles was from 2.1 (at *T* of -22°C) to 6.3 (at *T* of -15°C) times higher than that of fine particles. More specifically, the summer season AF at *T* of -22°C ranged from 2.0×10^{-5} to 3.2×10^{-4} for sub-micrometer aerosol particles and from 1.1×10^{-5} to 1.0×10^{-3} for super-micrometer ones. At *T* of -15°C, the AF values substantially increased as AF ranged from 1.2×10^{-6} to 9.8×10^{-5} for sub-micrometer aerosol particles and from 8.5×10^{-6} to 3.7×10^{-4} in the case of super-micrometer aerosol particles. The increasing trend of AF for super-micrometer fraction was not an exception in summer as it was also observed in spring season data, although to a lower extent. For instance, during spring time, the AF ranged from 1.5×10^{-5} to 1.9×10^{-4} for sub-micrometer aerosol particles and from 1.6×10^{-5} to 2.8×10^{-4} for super-micrometer one at *T* of -22°C. A similar trend was observed at -15°C: 1.4×10^{-6} - 2.2×10^{-5} (sub-micrometer aerosol subset) to 2×10^{-6} - 1.1×10^{-4} (super-micrometer aerosol particles).

Analogously, Si et al. (2018) and Creamean et al. (2018) reported a higher ice nucleation efficiency for super-micrometer particles sampled at Arctic stations. The above cited papers report data collected in both summer (Si et al., 2018) and spring (Creamean et al., 2018). In particular, Si et al. (2018) reported AF data in the range between 2×10^{-3} and ~8×10^{-2}, for super-micrometer particles at -25°C and about 10^{-4} for sub-micrometer sized particles at -20 and -25°C.

3.4 Seasonal variation in *n*INP and AF

Recent works reported a marked seasonal trend for *n*INP in the Arctic environment, with atmospheric loadings increasing from spring to summer time (Santl-Temkiv et al., 2019; Wex et al., 2019; Tobo et al., 2019). In particular, Wex et al. (2019) reported the increase in *n*INP of a factor of 10 times or more, at four Arctic sampling stations. The paper deals with measurements performed on aerosol particle samples collected from March 2012 to April 2016 with an inclusion of the GVB data limited to 2012 spring-summer. The reason of the observed seasonal *n*INP transition was not clear but presumed to be a contribution from local sources, both of mineral and biological particles, during the warm season after ice and snow melting (Santl-Temkiv

et al., 2019). Conversely, Schrod et al. (2020) showed no significant seasonal trend in *n*INP at the Zeppelin Observatory, located about 470 m above Ny-Ålesund, with a significantly larger data set with respect to the present study (almost continuous observations between May 2015 and January 2017).

Interestingly, our 2018 time series data in Fig. 4 do not indicate a clear seasonal increase in ambient *n*INP from spring to summer. A comparison between the seasonal trends in this study and from Wex et al. (2019) can be found in Fig. S3. For the DFPC data, a statistically significant ($p<0.01$) *n*INP reduction (by a factor 1.5) was found at *T* of -22°C, passing from the spring campaign (April) to the summer period (July), while no significant ($p>0.05$) difference was observed for *T*s of -15 and -18°C.

The time series of *n*INP measured by WT-CRAFT agrees with the DFPC one if we consider only the periods in which the two sampling activities were run in parallel: a statistically significant ($p<0.05$) reduction by a factor 1.6 is observed at -22°C and no significant differences can be appreciated at -15 and -18°C. On the other hand, considering the whole WT-CRAFT data extent, a statistically significant ($p<0.05$) increasing *n*INP seasonal trend was observed but only for *T*s between -17.5 and -21.5°C. Even in these cases, the spring to summer enhancement ratios did not exceeded a factor of three. We notice that such variations are smaller than the variability of *n*INP observed within one season. A primary peak in *n*INP was observed by WT-CRAFT during June, at *T*s lower than *T* = -17°C (Figs. 4a and 4b). Further, the increase was visually notable in this case: the average *n*INP during June was up to ~3 (*T* = -20°C) times higher than the average of the rest of the measurement period. As can be seen in Figs. 4a and 4b, a second peak of *n*INP can be observed at the end of the WT-CRAFT measurement period, with the last sample presenting the highest concentrations of all the campaign for many activation *T*s. Further discussion of the *n*INP-AF relationship during this specific period is provided below.

Both datasets show a general increase of the AF from spring to summer as shown in Fig. 5. DFPC showed a statistically significant ($p<0.02$) increase of the AF, passing from the spring campaign to the summer period for all the probed activation *T*s. The seasonal increase in the AF is more evident at higher *Ts*: the summer to spring mean ratio is 6.1 at *T* of -15°C and 2.5 at *T* of -22°C. Consistent results can be observed in the WT-CRAFT dataset. Comparing the first month of the campaign (16 April – 18 May) with the last month of the campaign (01 July – 02 August), an enhancement of AF (from 1.3 to 5.7 fold, considering the median ratios) can be observed for all the activation *T*s. This difference was statistically significant ($p<0.05$) for all the activation *T*s between -13.5 and -23°C. Differently from the DFPC data, the spring to summer AF increase from WT-CRAFT data had its maximum at *T* = -19°C (5.7), with the minimum value obtained at *T* = -25°C (1.4) (Fig. S4).

The AF time series by WT-CRAFT reported in Fig. 5 reflects the increase in *n*INP characterizing the month of June as described above. This demonstrates that the enhancement in *n*INP (for $T < -17$°C) observed in June was due to enhanced ice nucleation activity of the particle population (more INP per particle number), rather than to an increase of aerosol particle concentration. We note that the AF data of WT-CRAFT in August is not available due to the lack of SMPS-APS data (maintenance reason). Thus, whether the increase of *n*INP detected by WT-CRAFT in August (i.e., the last two data point sin Figs. 4a and 4b) corresponds to the enhancement of ice nucleation efficiency or absolute aerosol particle concentration remains uncertain.

3.5 Relation of *n*INP with meteorological parameters and particle number concentration

Analysing the patterns of the main meteorological parameters (*T*, pressure, RH, WS and precipitation) in relation to *n*INP, no clear relation emerges, with the exception of precipitation events, which were often associated to a reduction of *n*INP (Fig. S5). Although *n*INP tends to covariate with particle number concentration (in the range 0.5-10 µm) during the spring campaign (Pearson's R of 0.18, for INP_{PM10} at T= -22°C, and 0.22, for INP_{PM10} at *T* = -18°C), a significant correlation (R = 0.56; p< 0.05) was observed only for INP_{PM10} at *T* = -15°C, in the DFPC dataset. During summer, no correlation at all was observed between *n*INP and particle number (R between -0.13 and -0.25). For WT-CRAFT significant correlations (p<0.05) were observed only for T<-23°C (R between 0.42 and 0.52). It is, however, important to note that previous studies from different regions report various results about the correlation between INP and particle number concentration: a correlation is often reported with the number concentration of aerosol particles larger than 0.5 µm (DeMott et al., 2010; DeMott et al., 2015; Mason et al., 2015; Schwikowski et al., 1995); in other cases, a complete lack of correlation has been documented (Richardson et al., 2007; Rogers et al., 1998), which is not surprising considering that INPs are only a small fraction of total particles. Bigg (1996) reported a good correlation between *n*INP and accumulation mode particles, for one day of measurements over the high Arctic, while a modest but significant correlation (R = 0.25 – 0.30) between *n*INP and particle number concentration in the 50-120 nm range was reported by Bigg and Leck (2001), close to the North Pole. No other paper, to the best of our knowledge, addressed this relation in the Arctic environment.

3.6. Sources of INPs in the Arctic

3.6.1 Correlation with chemical tracers

In order to investigate the potential sources of the INPs at GVB, a correlation analysis was performed between both *n*INP datasets and the atmospheric concentration of chemical tracers routinely measured at the station. During the spring campaign, *n*INP correlated with tracers of long range transported anthropogenic aerosol particles such as nitrates, non-sea-salt-sulfate and non-sea-salt-potassium (Table 3). Indeed, Udisti et al. (2016) associated spring time non-sea-salt-sulfate at GVB to long range transported anthropogenic sources. The authors also showed that the production of biogenic non-sea-salt-sulfate from the sea is relevant only in summer time. The spring time peak of anthropogenic aerosol transport from lower latitudes is often referred to as the Artic haze (Shaw, 1995). A general tendency to anticorrelation with sodium and chlorine was also observed in both the size classes, though only PM_1 is statistically significant (p<0.05). The only significant relations observed from the analysis of the summer DFPC data was for *T* = -15°C: an anticorrelation was observed between $nINP_{PM10}$ and particulate mass, sea spray tracers (sodium and chlorine) and calcium, magnesium and lithium.

No clear source indications were derived from the correlation analysis of the WT-CRAFT data to the chemical tracers as a whole. However, analysing seasonally categorized $nINP_{WT\text{-}CRAFT}$ (spring and summer separation on May 31) resulted in a similar result found through the DFPC data (Table 4). In short, in spring season, $nINP_{WT\text{-}CRAFT}$ correlated with tracers of anthropogenic long-range transported aerosols (non-sea-salt-sulfate, nitrate, non-sea-salt-potassium), particularly at low

activation *T*s. Additionally, calcium concentration exhibied some tendency to correlate with *n*INP (both datasets). Whether it is from natural dust or other anthrophonic sources cannot be decided from our analysis, and it is not conclusive if it has any impact on *n*INP. In summer season, no significant correlation ($p<0.05$) was observed. One caution is that our tracer analysis only infers the aerosol properties, and further analysis of INP identities and properties (e.g., ice crystal residual analysis) would be necessary to reveal the source of INPs.

3.6.2 Influence of ground conditions

The influence of ground conditions (sea-ice, snow, seawater and land) on the examined low-travelling back-trajectories (<500m) was evaluated by merging back trajectories and satellite ground type data (Wex et al., 2019). Figure 6 shows that the contribution of the four considered ground types varies with the season. In spring, the majority of contacts occurred with sea-ice or snow-covered land, while in summer low air masses were more influenced by ice-free seawaters. The (snow-free) land contribution was the lowest in every season. Nevertheless, the influence of land sources on *n*INP emerges clearly from Table 5 and Fig. S6: air masses with a higher terrestrial influence were always associated with *n*INP peaks. This is probably due to the higher ice nucleation efficiency of mineral dust and soil particles compared to marine biological particles (Wilson et al., 2015; McCluskey et al., 2018a; McCluskey et al., 2018b). In summer, contacts with snow-free land occurred mainly within the Svalbard archipelago (local sources) or over Greenland and Iceland (regional sources), as shown in Fig. 6.

3.6.3 Contribution of marine biological INP sources

Considering that the sampled air masses had ground contacts mainly over seawater during summer, one can hypothesize that marine biological sources may dominate *n*INP at GVB, outside the periods of elevated terrestrial influence. To check this hypothesis, we investigated the spatio-temporal correlation of the INP datasets with satellite retrieved surface CHL, used as a tracer for marine biological activity, following the time-lag approach first introduced by Rinaldi et al. (2013). The DFPC dataset was selected to run this analysis because it provides a higher time resolution than the WT-CRAFT one and, most of all, because it allows to distinguish between fine and coarse INPs. In fact, McCluskey et al. (2018b) and Mansour et al. (2020b) showed that fine INPs tend to correlate better with CHL in clean marine air masses. To exclude interferences from land sources, we screened the samples corresponding to back trajectories that have been in contact with land for more than 10% of the time (3 samples) from the entire dataset. Furthermore, we focused on INP data obtained at *T* of -15°C, which are the most representative of ice nucleation by biological particles and the less subject to influences from mineral particles (Kanji et al., 2017).

The results of the correlation analysis are reported in Fig. 7, in the form of correlation maps. In the maps, the colour of each pixel represents the correlation coefficient (R) resulting from the linear regression between the CHL concentration in that pixel and $n\mathrm{INP}_{\mathrm{PM1}}$ measured at GVB. Different maps were obtained by considering different time-lags between the two correlated time series, i.e., by considering CHL concentration values shifted back in times of 1 to 27 days with respect to the INP filter sampling times (the maps are shown in Fig. S7). The time-lag approach has been demonstrated to maximize the correlation

between in situ coastal measurements of aerosol properties and CHL concentration fields (Rinaldi et al., 2013; Mansour et al., 2020b; Mansour et al., 2020a); it reflects the time scale of the biochemical processes responsible for the production of transferable organic matter in the seawater after the phytoplankton growing phase that is tracked by CHL patterns. Sea regions characterized by high correlation (red dots in the maps) are potentially related to the emission of biological particles acting as INPs in our samples. Figure 7 reports three examples of correlation maps, with time-lag 6, 14 and 16 days. The maps in Fig. 7 were selected because they clearly show high correlation regions in the seawaters surrounding the Svalbard archipelago (time-lag 6 days), close to the Greenland coast (time-lag 14 and 16 days) and to the northeast of Iceland (time-lag 16 days). These regions were all consistently located upwind GVB during the sampling period (Fig.6). All the obtained maps are available in the Supplementary Material, including those obtained with PM_{10} INP data, which as expected, do not evidence any significant correlation with CHL (Fig. S8). Considerations on the robustness of the correlation maps can be found in the Supplementary Material (Sect. S1 and Figs. S9-S11). In our interpretation, the lack of a correlation between surface CHL concentration and coarse INPs does not imply that coarse INPs are not emitted from the ocean surface, it simply evidences that CHL is not the appropriate proxy to track the emission of large biological INP from the oceans. Indeed, CHL has been previously observed to correlate with the enrichment of organic matter in sub-micron sea spray (Rinaldi et al., 2013; O'Dowd et al., 2015) but no investigation was ever attempted with super-micrometer particles. In a laboratory-controlled setting, McCluskey et al. (2017) evidenced the production of both sub- and super-micrometer INPs during laboratory experiments at around -22°C with controlled algal blooms, pointing out that different particle type and production mechanisms are involved. However, the discussions regarding the relationship and time lag between chlorophyll production and sea spray aerosols generation in the atmosphere, and subsequent ambient INP identification from the chlorophyll source, are still under debate as these represent complex processes over an oceanic-atmospheric interface over a wide spatiotemporal scale (Crocker et al., 2020; Wolf et al., 2021; Mansour et al., 2020b).

Our correlations alone cannot imply unambiguously a cause-effect relation, therefore we also run the CWT spatial source attribution model on the same INP dataset (DFPC; PM_1; T = -15° C; no land influenced samples). The resulting map (Fig. 8a), composed of 203 cells over the selected domain, evidences that potential sub-micron INP sources at GVB, during the summer period, were broadly located in the same sea regions previously evidenced by the spatio-temporal correlation with CHL. In order to facilitate the comparison between spatio-temporal correlation maps and the CWT results, we have evidenced each pixel that has both a high CWT value (defined as above the median), and a significant and positive correlation between $n\mathrm{INP}_{PM1}$ and surface CHL, considering every delay time between 5 and 20 days (Fig. 8b). The sea regions close to Svalbard and immediately to the East of Greenland are clearly evidenced by this analysis, suggesting that they may have been involved in the emission of biogenic INPs sampled at GVB, outside the major evidenced episodes of terrestrial influence. The combined analysis also suggests that the region in the northeast of Iceland may also be a potential bio INP source area, even though the spatial distribution of the evidenced pixels is more scattered and, therefore, less convincing.

4. Discussion

4.1. Interpretation of $n\mathrm{INP}_{\mathrm{DFPC}}$ and $n\mathrm{INP}_{\mathrm{WT\text{-}CRAFT}}$: condensation vs. immersion freezing

The difference between $n\mathrm{INP}_{\mathrm{DFPC}}$ and $n\mathrm{INP}_{\mathrm{WT\text{-}CRAFT}}$ reported in Sect. 3.1 may derive from the different time intervals of aerosol particle samplings for the two techniques, the uncertainties in sampling activities (e.g., size-dependant collection efficiency), suppression of INPs over time (Beall et al., 2020), measurement uncertainties or a combination of any. We discuss the contribution of each factor on causing potential offset between $n\mathrm{INP}_{\mathrm{DFPC}}$ and $n\mathrm{INP}_{\mathrm{WT\text{-}CRAFT}}$ below.

The overall uncertainties of individual ice nucleation measurements cannot explain entirely the observed discrepancy, particularly at T of -15°C, where more than one half of the discrepancy remains unexplained. Furthermore, systematic uncertainties in the sampling procedures, as a bias in the sampled volumes, cannot justify a T-dependent concentration discrepancy as the one discussed here.

The PM_1 and PM_{10} sampling inlet systems used for DFPC are certified with 100% collection efficiency at the employed flow rates. Similarly, the collection efficiency of sub-micron aerosol particles (tested using 200-300 nm mode test mineral dust particles) through the 47 mm filter sampler for WT-CRAFT is virtually 100%. For super-micron population, its sampling efficiency somehow decreases to ~70% (tested with 2-3 µm test fibrous particles) presumably because the test particles stack inside the sampler inlet and/or a filter holder wall. We cannot rule out the impact of particle losses on $n\mathrm{INP}_{\mathrm{WT\text{-}CRAFT}}$ and resulting deviation from $n\mathrm{INP}_{\mathrm{DFPC}}$ especially under the conditions where super-micron, coarse INPs prevail (i.e., up to 32% and 65% at -15 °C in spring and summer, respectively, according to Table 2). But, as inferred in Figs. 2-4, there is no systematic increase in the deviation between $n\mathrm{INP}_{\mathrm{WT\text{-}CRAFT}}$ and $n\mathrm{INP}_{\mathrm{DFPC}}$ from spring to summer season while the gap between $n\mathrm{INP}_{\mathrm{WT\text{-}CRAFT}}$ and $n\mathrm{INP}_{\mathrm{DFPC}}$ is expected to be diverse in summer season (and towards high T) if the loss of super-micron aerosol particles during the sampling affect $n\mathrm{INP}_{\mathrm{WT\text{-}CRAFT}}$. As we do not observe any strong indications of these influence within given uncertainties, it is at least conclusive that the size-dependant collection efficiency of aerosol particles is not a solo-dominating factor causing the difference between $n\mathrm{INP}_{\mathrm{WT\text{-}CRAFT}}$ and $n\mathrm{INP}_{\mathrm{DFPC}}$.

Beall et al. (2020) recently reported a decrease in nINP up to approximately 42% is possible when stored at 4 °C and suggested correction factors at -17°C < T < -7°C. However, as we kept the samples for DFPC at the room air T (and the WT-CRAFT samples at 4 °C except during transportation), the suppression of INPs due to the sample storage difference does not explain the observed general trend of $n\mathrm{INP}_{\mathrm{DFPC}} > n\mathrm{INP}_{\mathrm{WT\text{-}CRAFT}}$.

In this study, we are comparing samples collected over different time periods (~4 hours for the DFPC and ~4 days for WT-CRAFT). Although we cannot exclude the possibility that short episodes of high INPs-containing air masses increased $n\mathrm{INP}_{\mathrm{DFPC}}$, this is unlikely for two reasons: (1) a systematic difference, as that object of this discussion, would presume a strong nINP daily trend with the maximum coinciding with the DFPC sampling time. This was excluded by analysing the daily evolution of the particle number concentration, which does not present any evident diurnal trend both in spring and summer; (2) the general AF time series (Fig. 4) almost consistently show $\mathrm{AF}_{\mathrm{DFPC}} > \mathrm{AF}_{\mathrm{WT\text{-}CRAFT}}$ over two seasons; this suggests that the

higher *n*INP for DFPC samples results from higher ice activation at the conditions of DFPC analyses rather than from higher aerosol particle number concentration in DFPC samples.

Besides the factors discussed above, the fact that the $AF_{DFPC,PM1}$ values often exceeded $AF_{WT\text{-}CRAFT}$ (total aerosol particles through a TSP inlet) in Fig. 4 also suggest that the unexplained concentration gap might stem from other factors, and it is plausible to consider a different sensitivity of Arctic INPs to different ice nucleation modes. Indeed, in condensation mode measurements, water vapor condenses on the surface of sampled aerosol particles, possibly coated with soluble compounds. In the case of immersion freezing measurements, water soluble compounds are dissolved in the suspension water, leaving the insoluble nuclei uncoated or with a modified coating in the analysed water droplets. This can alter the physicochemical properties of the aerosol particle surface as well as their freezing efficiency. A detailed intercomparison of techniques is not under the scope of this study. However, our past attempts to intercompare DFPC and WT-CRAFT measurements with different aerosol types yielded different results. For instance, the analyses of microcrystalline and fibrous cellulose samples showed that DFPC tended to form more ice crystals than WT-CRAFT (Hiranuma et al., 2019), while the analyses of ambient continental aerosol particles, collected by identical sampling systems as used in this study, from the Po Valley resulted in equivalent or higher ice crystal numbers in WT-CRAFT (not shown as the data is unpublished). These observed variations in the *n*INP comparability at least suggest some sensitivity of the aerosol particle type to the different ice activation modes (and vice versa). Nevertheless, we considered that our INP detection techniques are within a reasonable agreement, according to the overall uncertainty of a subset of existing INP measurement techniques in a recent intercomparison study (DeMott et al., 2017; Hiranuma et al., 2019).

4.2. Interpretation of seasonal variability of *n*INP

In 2018, we observed seasonal variation depending on the activation *T*. In short, within a limited range of *T*s (-17.5 to -21.5°C), our $nINP_{WT\text{-}CRAFT}$ exhibited statistically significant variations. But, the overall $nINP_{WT\text{-}CRAFT}$ at any lower *T*s peaked during the month of June (up to 3 times higher concentration that the rest of the sampling period). A similar observation of insignificant seasonal *n*INP trends from Ny-Ålesund is reported in Schrod et al. (2020). The observed discrepancy between current and aforementioned past studies may be indicative of the inter-annual variability of meteorological conditions and aerosol particle sources determining the ambient *n*INP. Nonetheless, the number of *n*INP observations in the Arctic and their temporal coverage remains too limited to derive conclusive interpretation of the *n*INP seasonal trends. Future application of long-term online INP measurements (e.g., Möhler et al. (2021)) may allow shedding light on the seasonal evolution of *n*INP at GVB and over the Arctic in general.

The analysis of the AF evidences generally more notable seasonal trends, with both techniques showing a statistically significant increase in the ice nucleation capability of atmospheric aerosol particles passing from spring to summer. The chemical tracer correlation analysis, the ground contribution analysis and the above presented considerations on the different contributions of sub- and super-micrometer INPs in spring and summer time suggest that the main sources of spring time INPs measured at GVB may be located outside the Arctic. They are deemed to derive from the lower latitude regions together with

anthropogenic aerosols during the Artic haze (Heidam et al., 1999; Stohl, 2006). Conversely, the summer time aerosol particles population is more related to local (Arctic) sources. These results evidence that long-range transported aerosol particles from lower latitudes have a lower ability in nucleating ice than aerosol particles originating from local sources, dominant during summer time. This is in agreement with the findings by Hartmann et al. (2019), which showed a low impact of anthropogenic emissions on Arctic *n*INP, by comparing present-day and pre-industrial *n*INP values through the analysis of ice core records. We notice that, although the correlation with chemical tracers suggests a common spatial origin for spring time INPs and anthropogenic aerosol particles, we are not able to assess to which extent anthropogenic aerosol particles contributed to the observed spring time INP loads.

The higher ice nucleation efficiency of summer time (local) aerosol particles may be related to different physico-chemical properties of spring vs. summertime aerosol particles at GVB but also to the enhanced contribution of super-micrometer aerosol particles during summer time, reported to be more ice nucleation active in this and previous studies. Addressing which of these two factors is more influential over the Arctic would be an interesting subject for further investigations.

4.3. Sources of INPs at GVB

Our analysis points out that both marine and terrestrial sources may contribute to the INP population in the study area, with land sources showing a potential for dominating the INP pool, due to the higher ice activity of mineral dust and soil particles. On the contrary, marine sources may be significant, even though marine INPs are intrinsically less ice active, because of the extension of ice-free sea waters during the Arctic summer. This has implications also for the future balance between terrestrial and marine INP sources in a warming Arctic (Murray et al., 2021). The major limitation of our spatio-temporal correlation analysis and of the INP spatial source attribution approach (CWT) is the low number of samples available. This limits the time representativeness of the dataset and increases the uncertainty of the outputs. Nevertheless, the consistency of the two independent approaches (spatio-temporal correlation analysis and CWT source location) provides a certain measure of credibility to the presented results. For this reason, we consider the above as an implication that the marine biota may be a source of INPs in the Arctic. Nevertheless, further studies, based on more robust datasets, are necessary to confirm this result and to achieve a more quantitative understanding of the relative importance of marine vs. terrestrial INP sources over the Arctic. In particular, online INP quantification methods have the potential to provide better suitable data for this kind of statistical approaches and will certainly contribute to clarify INP sources over the Arctic in the future.

5 Conclusions

This work presented the ambient concentration of INPs using offline immersion and condensation freezing techniques on aerosol particle samples collected from the GVB observatory, near Ny-Ålesund, during spring-summer 2018. The *n*INP values measured by DFPC ranged 33-185, 5-107 and 3-66 m^{-3}, for *Ts* of -22, -18 and -15°C, respectively. At the same activation *T*s, WT-CRAFT measured 3-199, 1-34 and 1-4 m^{-3}. Although the two sets of data presented a fair agreement in terms of *n*INP

trends, a notable offset is evident, with the DFPC generally presenting higher *n*INPs than the WT-CRAFT. This offset increases with *T*, resulting in a factor of 8 at *T* of -15°C. We considered many factors that could potentially explain the observed difference (Sect. 4) and conclude that the different ice nucleation mechanisms probed by the two techniques (condensation freezing, for DFPC, and immersion freezing, for WT-CRAFT) is an undeniable reason. While differences in the sampling resolution and overall measurement uncertainties have partly contributed to the observed offset, it seems conclusive to address there is ice nucleation mode dependent INP propensity at GVB in 2018 at least. Any future investigations regarding INP compositions and more controlled-study focusing on condensation vs. immersion freezing on identified compositions will lead to further findings to settle this issue.

This study also offered unique data examining the seasonality of INPs in the Arctic with respect to *n*INP and AF. Both condensation and immersion INP datasets did not indicate a marked *n*INP seasonal trend. We report a statistically significant spring to summer enhancement in *n*INP only for a narrow range of *Ts* (-17.5 to -21.5°C) and the associated *n*INP enhancement never exceeded a factor of three. On the other hand, the AF of atmospheric aerosol particles from GVB presents a statistically significant spring to summer increase almost independent on the probed *T*, reaching up to ca. 6 times at *T* of -19°C. A clear seasonal evolution of the super-micrometer INP contribution was observed by DFPC. Such contribution was around 20% in spring (with the highest 32% at -15 °C) and increasing markedly in summer and at high *Ts* (45% at *T* of -22°C and 65% at *T* of -15°C). This implies an important role of super-micrometer aerosol particles as the source of summer time Arctic INPs. Additionally, our chemical tracer and back-trajectory analyses shows the dominance of local aerosol particle sources during summer and the influence of anthropogenic sources in spring. In short, the summer season ground conditions influenced the sampled air masses, suggesting that the summer time INP population are influenced by terrestrial and marine sources. Our summer season analysis also indicated a relationship between the biological activity in specific seawater regions and *n*INP at the sampling point. On the other hand, the INP spring time population at GVB is mostly influenced by long range transport of aerosol particles from lower latitudes. Spring season air masses are characterized by markers of anthropogenic aerosol particles. Determining if such anthropogenic particles contribute to the observed INP loads is beyond the scope of the current study, but the future study of anthropogenic vs. natural INPs in the Arctic region by assessing detailed INP composition will be an important step to comprehensively understand the impact of INPs in the Arctic cloud formation, precipitation and climate.

6 Data availability

Data discussed in this work are available at http://dx.doi.org/10.17632/zf4wdcc3bw.1

Satellite Chlorophyll data are available for download at http://marine.copernicus.eu/ (product identifier: OCEANCOLOUR_GLO_CHL_L4_REP_OBSERVATIONS_009_082).

7 Author contribution

MR, NH, and FB designed the concept of this collaborative research. MR led the overall manuscript writing effort with support of all authors. Methodology was developed by GS, FB, and NH, and measurements were conducted by GS, FB, CAR, MM, DC, SB, RT, and MP. Formal data analyses were carried out by MR, NH, FB, and KM. The revision effort was led by MR and NH with support of all authors.

8 Competing interests.

The authors declare that they have no conflict of interest.

9 Acknowledgements

The authors thank DSSTTA-CNR and its staff for the logistical support that allowed the realization of the experimental activity. This activity was funded by the H2020 EU Project FORCeS (Constrained aerosol forcing for improved climate projections; Grant agreement ID: 821205). Francescopiero Calzolari is greatly acknowledged for his support to the maintenance of the DFPC.

N. Hiranuma and C. A. Rodriguez acknowledges contributions of H.S. Vepuri, Y. Hou and Z. Salcido for their technical support on WT-CRAFT measurements. N. Hiranuma thanks for the funding support from Killgore Faculty Research Grant and the WTAMU's IoT and Research Computing program. N. Hiranuma also acknowledges partial financial support by Higher Education Assistance Fund (HEAF). This material is based upon work supported by the National Science Foundation under Grant No. 1941317 (CAREER: The Role of Ice-Nucleating Particles and Their Feedback on Clouds in Warming Arctic Climate). The authors acknowledge the NySMAC, Ny-Ålesund Atmosphere Research Flagship Programme, for allowing the organization of a collaborative workshop meeting held in Bologna, Italy, in 2017. The workshop provided a venue for authors to come together that fostered this collaboration.

References

Atkinson, J. D., Murray, B. J., Woodhouse, M. T., Whale, T. F., Baustian, K. J., Carslaw, K. S., Dobbie, S., O'Sullivan, D., and Malkin, T. L.: The importance of feldspar for ice nucleation by mineral dust in mixed-phase clouds, Nature, 498, 355-358, 10.1038/nature12278, 2013.

Beall, C. M., Lucero, D., Hill, T. C., DeMott, P. J., Stokes, M. D., and Prather, K. A.: Best practices for precipitation sample storage for offline studies of ice nucleation in marine and coastal environments, Atmospheric Measurement Techniques, 13, 6473-6486, 10.5194/amt-13-6473-2020, 2020.

Becagli, S., Ghedini, C., Peeters, S., Rottiers, A., Traversi, R., Udisti, R., Chiari, M., Jalba, A., Despiau, S., Dayan, U., and Temara, A.: MBAS (Methylene Blue Active Substances) and LAS (Linear Alkylbenzene Sulphonates) in Mediterranean coastal aerosols: Sources and transport processes, Atmospheric Environment, 45, 6788-6801, 10.1016/j.atmosenv.2011.04.041, 2011.

Belosi, F., Piazza, M., Nicosia, A., and Santachiara, G.: Influence of supersaturation on the concentration of ice nucleating particles, Tellus Series B-Chemical and Physical Meteorology, 70, 10.1080/16000889.2018.1454809, 2018.

Belosi, F., Rinaldi, M., Decesari, S., Tarozzi, L., Nicosia, A., and Santachiara, G.: Ground level ice nuclei particle measurements including Saharan dust events at a Po Valley rural site (San Pietro Capofiume, Italy), Atmospheric Research, 186, 116-126, 10.1016/j.atmosres.2016.11.012, 2017.

Bergeron, T.: On the Physics of clouds and precipitation, in: Proces Verbaux de l'Association de Meteorologie, 156-178, International Union of Geodesy and Geophysics, 1935.

Bigg, E. K.: Ice forming nuclei in the high Arctic, Tellus Series B-Chemical and Physical Meteorology, 48, 223-233, 10.1034/j.1600-0889.1996.t01-1-00007.x, 1996.

Bigg, E. K. and Leck, C.: Cloud-active particles over the central Arctic Ocean, Journal of Geophysical Research-Atmospheres, 106, 32155-32166, 10.1029/1999jd901152, 2001.

Borys, R. D.: The effects of long-range transport of air pollutants on Arctic cloud-active aerosol, Atmospheric Science, Colorado State University, Fort Collins, Colorado, USA, 367 pp., 1983.

Buck, A. L.: NEW EQUATIONS FOR COMPUTING VAPOR-PRESSURE AND ENHANCEMENT FACTOR, Journal of Applied Meteorology, 20, 1527-1532, 10.1175/1520-0450(1981)020<1527:nefcvp>2.0.co;2, 1981.

Conen, F., Stopelli, E., and Zimmermann, L.: Clues that decaying leaves enrich Arctic air with ice nucleating particles, Atmospheric Environment, 129, 91-94, 10.1016/j.atmosenv.2016.01.027, 2016.

Creamean, J. M., Kirpes, R. M., Pratt, K. A., Spada, N. J., Maahn, M., de Boer, G., Schnell, R. C., and China, S.: Marine and terrestrial influences on ice nucleating particles during continuous springtime measurements in an Arctic oilfield location, Atmospheric Chemistry and Physics, 18, 18023-18042, 10.5194/acp-18-18023-2018, 2018.

Crocker, D. R., Hernandez, R. E., Huang, H. D., Pendergraft, M. A., Cao, R. C., Dai, J. Y., Morris, C. K., Deane, G. B., Prather, K. A., and Thiemens, M. H.: Biological Influence on $\delta^{13}C$ and Organic Composition of Nascent Sea Spray Aerosol, Acs Earth and Space Chemistry, 4, 1686-1699, 10.1021/acsearthspacechem.0c00072, 2020.

de Boer, G., Shupe, M. D., Caldwell, P. M., Bauer, S. E., Persson, O., Boyle, J. S., Kelley, M., Klein, S. A., and Tjernstrom, M.: Near-surface meteorology during the Arctic Summer Cloud Ocean Study (ASCOS): evaluation of reanalyses and global climate models, Atmospheric Chemistry and Physics, 14, 427-445, 10.5194/acp-14-427-2014, 2014.

DeMott, P. J., Prenni, A. J., Liu, X., Kreidenweis, S. M., Petters, M. D., Twohy, C. H., Richardson, M. S., Eidhammer, T., and Rogers, D. C.: Predicting global atmospheric ice nuclei distributions and their impacts on climate, Proceedings of the National Academy of Sciences of the United States of America, 107, 11217-11222, 10.1073/pnas.0910818107, 2010.

DeMott, P. J., Prenni, A. J., McMeeking, G. R., Sullivan, R. C., Petters, M. D., Tobo, Y., Niemand, M., Mohler, O., Snider, J. R., Wang, Z., and Kreidenweis, S. M.: Integrating laboratory and field data to quantify the immersion freezing ice nucleation activity of mineral dust particles, Atmospheric Chemistry and Physics, 15, 393-409, 10.5194/acp-15-393-2015, 2015.

DeMott, P. J., Hill, T. C. J., Petters, M. D., Bertram, A. K., Tobo, Y., Mason, R. H., Suski, K. J., McCluskey, C. S., Levin, E. J. T., Schill, G. P., Boose, Y., Rauker, A. M., Miller, A. J., Zaragoza, J., Rocci, K., Rothfuss, N. E., Taylor, H. P., Hader, J. D., Chou, C., Huffman, J. A., Poschl, U., Prenni, A. J., and Kreidenweis, S. M.: Comparative measurements of ambient atmospheric concentrations of ice nucleating particles using multiple immersion freezing methods and a continuous flow diffusion chamber, Atmospheric Chemistry and Physics, 17, 11227-11245, 10.5194/acp-17-11227-2017, 2017.

Dymarska, M., Murray, B. J., Sun, L. M., Eastwood, M. L., Knopf, D. A., and Bertram, A. K.: Deposition ice nucleation on soot at temperatures relevant for the lower troposphere, Journal of Geophysical Research-Atmospheres, 111, 10.1029/2005jd006627, 2006.

Findeisen, W.: Kolloid-Meteorologische, American Meteorological Society, 2nd Edn., 1938.

Giardi, F., Becagli, S., Traversi, R., Frosini, D., Severi, M., Caiazzo, L., Ancillotti, C., Cappelletti, D., Moroni, B., Grotti, M., Bazzano, A., Lupi, A., Mazzola, M., Vitale, V., Abollino, O., Ferrero, L., Bolzacchini, E., Viola, A., and Udisti, R.: Size distribution and ion composition of aerosol collected at Ny-lesund in the spring-summer field campaign 2013, Rendiconti Lincei-Scienze Fisiche E Naturali, 27, 47-58, 10.1007/s12210-016-0529-3, 2016.

Hande, L. B. and Hoose, C.: Partitioning the primary ice formation modes in large eddy simulations of mixed-phase clouds, Atmospheric Chemistry and Physics, 17, 14105-14118, 10.5194/acp-17-14105-2017, 2017.

Harrington, J. Y. and Olsson, P. Q.: On the potential influence of ice nuclei on surface-forced marine stratocumulus cloud dynamics, Journal of Geophysical Research-Atmospheres, 106, 27473-27484, 10.1029/2000jd000236, 2001.

Harrington, J. Y., Reisin, T., Cotton, W. R., and Kreidenweis, S. M.: Cloud resolving simulations of Arctic stratus - Part II: Transition-season clouds, Atmospheric Research, 51, 45-75, 10.1016/s0169-8095(98)00098-2, 1999.

Hartmann, M., Blunier, T., Brugger, S. O., Schmale, J., Schwikowski, M., Vogel, A., Wex, H., and Stratmann, F.: Variation of Ice Nucleating Particles in the European Arctic Over the Last Centuries, Geophysical Research Letters, 46, 4007-4016, 10.1029/2019gl082311, 2019.

Heidam, N. Z., Wahlin, P., and Christensen, J. H.: Tropospheric gases and aerosols in northeast Greenland, Journal of the Atmospheric Sciences, 56, 261-278, 10.1175/1520-0469(1999)056<0261:tgaain>2.0.co;2, 1999.

Helfrich, S. R., McNamara, D., Ramsay, B. H., Baldwin, T., and Kasheta, T.: Enhancements to, and forthcoming developments in the Interactive Multisensor Snow and Ice Mapping System (IMS), Hydrological Processes, 21, 1576-1586, 10.1002/hyp.6720, 2007.

Hiranuma, N., Mohler, O., Yamashita, K., Tajiri, T., Saito, A., Kiselev, A., Hoffmann, N., Hoose, C., Jantsch, E., Koop, T., and Murakami, M.: Ice nucleation by cellulose and its potential contribution to ice formation in clouds, Nature Geoscience, 8, 273-277, 10.1038/ngeo2374, 2015.

Hiranuma, N., Adachi, K., Bell, D. M., Belosi, F., Beydoun, H., Bhaduri, B., Bingemer, H., Budke, C., Clemen, H. C., Conen, F., Cory, K. M., Curtius, J., DeMott, P. J., Eppers, O., Grawe, S., Hartmann, S., Hoffmann, N., Hohler, K., Jantsch, E., Kiselev, A., Koop, T., Kulkarni, G., Mayer, A., Murakami, M., Murray, B. J., Nicosia, A., Petters, M. D., Piazza, M., Polen, M., Reicher, N., Rudich, Y., Saito, A., Santachiara, G., Schiebel, T., Schill, G. P., Schneider, J., Segev, L., Stopelli, E., Sullivan, R. C., Suski, K., Szakall, M., Tajiri, T., Taylor, H., Tobo, Y., Ullrich, R., Weber, D., Wex, H., Whale, T. F., Whiteside, C. L., Yamashita, K., Zelenyuk, A., and Mohler, O.: A comprehensive characterization of ice nucleation by three different types of cellulose particles immersed in water, Atmospheric Chemistry and Physics, 19, 4823-4849, 10.5194/acp-19-4823-2019, 2019.

Hoose, C. and Mohler, O.: Heterogeneous ice nucleation on atmospheric aerosols: a review of results from laboratory experiments, Atmospheric Chemistry and Physics, 12, 9817-9854, 10.5194/acp-12-9817-2012, 2012.

Hsu, Y. K., Holsen, T. M., and Hopke, P. K.: Comparison of hybrid receptor models to locate PCB sources in Chicago, Atmospheric Environment, 37, 545-562, 10.1016/s1352-2310(02)00886-5, 2003.

Irish, V. E., Hanna, S. J., Willis, M. D., China, S., Thomas, J. L., Wentzell, J. J. B., Cirisan, A., Si, M., Leaitch, W. R., Murphy, J. G., Abbatt, J. P. D., Laskin, A., Girard, E., and Bertram, A. K.: Ice nucleating particles in the marine boundary layer in the Canadian Arctic during summer 2014, Atmospheric Chemistry and Physics, 19, 1027-1039, 10.5194/acp-19-1027-2019, 2019.

Jeong, U., Kim, J., Lee, H., Jung, J., Kim, Y. J., Song, C. H., and Koo, J. H.: Estimation of the contributions of long range transported aerosol in East Asia to carbonaceous aerosol and PM concentrations in Seoul, Korea using highly time resolved measurements: a PSCF model approach, Journal of Environmental Monitoring, 13, 1905-1918, 10.1039/c0em00659a, 2011.

Jiang, H. L., Cotton, W. R., Pinto, J. O., Curry, J. A., and Weissbluth, M. J.: Cloud resolving simulations of mixed-phase Arctic stratus observed during BASE: Sensitivity to concentration of ice crystals and large-scale heat and moisture advection, Journal of the Atmospheric Sciences, 57, 2105-2117, 10.1175/1520-0469(2000)057<2105:crsomp>2.0.co;2, 2000.

Kanji, Z. A., Ladino, L. A., Wex, H., Boose, Y., Burkert-Kohn, M., Cziczo, D. J., and Kramer, M.: Overview of Ice Nucleating Particles, Ice Formation and Evolution in Clouds and Precipitation: Measurement and Modeling Challenges, 58, 10.1175/amsmonographs-d-16-0006.1, 2017.

Knopf, D. A., Alpert, P. A., Wang, B., and Aller, J. Y.: Stimulation of ice nucleation by marine diatoms, Nature Geoscience, 4, 88-90, 10.1038/ngeo1037, 2011.

Lisok, J., Markowicz, K. M., Ritter, C., Makuch, P., Petelski, T., Chilinski, M., Kaminski, J. W., Becagli, S., Traversi, R., Udisti, R., Rozwadowska, A., Jefimow, M., Markuszewski, P., Neuber, R., Pakszys, P., Stachlewska, I. S., Struzewska, J., and Zielinski, T.: 2014 iAREA campaign on aerosol in Spitsbergen - Part 1: Study of physical and chemical properties, Atmospheric Environment, 140, 150-166, 10.1016/j.atmosenv.2016.05.051, 2016.

Lupi, A., Busetto, M., Becagli, S., Giardi, F., Lanconelli, C., Mazzola, M., Udisti, R., Hansson, H. C., Henning, T., Petkov, B., Strom, J., Krejci, R., Tunved, P., Viola, A. P., and Vitale, V.: Multi-seasonal ultrafine aerosol particle number concentration measurements at the Gruvebadet observatory, Ny-lesund, Svalbard Islands, Rendiconti Lincei-Scienze Fisiche E Naturali, 27, 59-71, 10.1007/s12210-016-0532-8, 2016.

Mansour, K., Decesari, S., Bellacicco, M., Marullo, S., Santoleri, R., Bonasoni, P., Facchini, M. C., Ovadnevaite, J., Ceburnis, D., O'Dowd, C., and Rinaldi, M.: Particulate methanesulfonic acid over the central Mediterranean Sea: Source region identification and relationship with phytoplankton activity, Atmospheric Research, 237, 10.1016/j.atmosres.2019.104837, 2020a.

Mansour, K., Decesari, S., Facchini, M. C., Belosi, F., Paglione, M., Sandrini, S., Bellacicco, M., Marullo, S., Santoleri, R., Ovadnevaite, J., Ceburnis, D., O'Dowd, C., Roberts, G., Sanchez, K., and Rinaldi, M.: Linking Marine Biological Activity to Aerosol Chemical Composition and Cloud-Relevant Properties Over the North Atlantic Ocean, Journal of Geophysical Research-Atmospheres, 125, 10.1029/2019jd032246, 2020b.

Mason, R. H., Si, M., Li, J., Chou, C., Dickie, R., Toom-Sauntry, D., Pohlker, C., Yakobi-Hancock, J. D., Ladino, L. A., Jones, K., Leaitch, W. R., Schiller, C. L., Abbatt, J. P. D., Huffman, J. A., and Bertram, A. K.: Ice nucleating particles at a coastal marine boundary layer site: correlations with aerosol type and meteorological conditions, Atmospheric Chemistry and Physics, 15, 12547-12566, 10.5194/acp-15-12547-2015, 2015.

Mason, R. H., Si, M., Chou, C., Irish, V. E., Dickie, R., Elizondo, P., Wong, R., Brintnell, M., Elsasser, M., Lassar, W. M., Pierce, K. M., Leaitch, W. R., MacDonald, A. M., Platt, A., Toom-Sauntry, D., Sarda-Esteve, R., Schiller, C. L., Suski, K. J., Hill, T. C. J., Abbatt, J. P. D., Huffman, J. A., DeMott, P. J., and Bertram, A. K.: Size-resolved measurements of ice-nucleating particles at six locations in North America and one in Europe, Atmospheric Chemistry and Physics, 16, 1637-1651, 10.5194/acp-16-1637-2016, 2016.

Mazzola, M., Viola, A. P., Lanconelli, C., and Vitale, V.: Atmospheric observations at the Amundsen-Nobile Climate Change Tower in Ny-lesund, Svalbard, Rendiconti Lincei-Scienze Fisiche E Naturali, 27, 7-18, 10.1007/s12210-016-0540-8, 2016.

McCluskey, C. S., Hill, T. C. J., Sultana, C. M., Laskina, O., Trueblood, J., Santander, M. V., Beall, C. M., Michaud, J. M., Kreidenweis, S. M., Prather, K. A., Grassian, V., and DeMott, P. J.: A Mesocosm Double Feature: Insights into the Chemical Makeup of Marine Ice Nucleating Particles, Journal of the Atmospheric Sciences, 75, 2405-2423, 10.1175/jas-d-17-0155.1, 2018a.

McCluskey, C. S., Ovadnevaite, J., Rinaldi, M., Atkinson, J., Belosi, F., Ceburnis, D., Marullo, S., Hill, T. C. J., Lohmann, U., Kanji, Z. A., O'Dowd, C., Kreidenweis, S. M., and DeMott, P. J.: Marine and Terrestrial Organic Ice-Nucleating Particles in Pristine Marine to Continentally Influenced Northeast Atlantic Air Masses, Journal of Geophysical Research-Atmospheres, 123, 6196-6212, 10.1029/2017jd028033, 2018b.

McCluskey, C. S., Hill, T. C. J., Malfatti, F., Sultana, C. M., Lee, C., Santander, M. V., Beall, C. M., Moore, K. A., Cornwell, G. C., Collins, D. B., Prather, K. A., Jayarathne, T., Stone, E. A., Azam, F., Kreidenweis, S. M., and DeMott, P. J.: A Dynamic Link between Ice Nucleating Particles Released in Nascent Sea Spray Aerosol and Oceanic Biological Activity during Two Mesocosm Experiments, Journal of the Atmospheric Sciences, 74, 151-166, 10.1175/jas-d-16-0087.1, 2017.

Murray, B. J., Carslaw, K. S., and Field, P. R.: Opinion: Cloud-phase climate feedback and the importance of ice-nucleating particles, Atmospheric Chemistry and Physics, 21, 665-679, 10.5194/acp-21-665-2021, 2021.

Murray, B. J., O'Sullivan, D., Atkinson, J. D., and Webb, M. E.: Ice nucleation by particles immersed in supercooled cloud droplets, Chemical Society Reviews, 41, 6519-6554, 10.1039/c2cs35200a, 2012.

Möhler, O., Adams, M., Lacher, L., Vogel, F., Nadolny, J., Ullrich, R., Boffo, C., Pfeuffer, T., Hobl, A., Weiß, M., Vepuri, H. S. K., Hiranuma, N., and Murray, B. J.: The Portable Ice Nucleation Experiment (PINE): a new online instrument for laboratory studies and automated long-term field observations of ice-nucleating particles, Atmospheric Measurement Techniques, 14, 1143-1166, 10.5194/amt-14-1143-2021, 2021.

National Ice-Center, U. S.: *IMS Daily Northern Hemisphere Snow and Ice Analysis at 1 km, 4 km, and 24 km Resolutions, Version 1*, Boulder , Colorado USA. NSIDC: National Snow and Ice Data Center [dataset], https://doi.org/10.7265/N52R3PMC, 2008.

O'Dowd, C., Ceburnis, D., Ovadnevaite, J., Bialek, J., Stengel, D. B., Zacharias, M., Nitschke, U., Connan, S., Rinaldi, M., Fuzzi, S., Decesari, S., Facchini, M. C., Marullo, S., Santoleri, R., Dell'Anno, A., Corinaldesi, C., Tangherlini, M., and Danovaro, R.: Connecting marine productivity to sea-spray via nanoscale biological processes: Phytoplankton Dance or Death Disco?, Scientific Reports, 5, 10.1038/srep14883, 2015.

Pinto, J. O.: Autumnal mixed-phase cloudy boundary layers in the Arctic, Journal of the Atmospheric Sciences, 55, 2016-2038, 10.1175/1520-0469(1998)055<2016:ampcbl>2.0.co;2, 1998.

Pruppacher, H. R., and Klett, J. D.: Heterogeneous Nucleation. In Microphysics of Clouds and Precipitation – Second Revised and Enlarged Edition, pp. 287-360, Springer, 2010.

Rangno, A. L. and Hobbs, P. V.: Ice particles in stratiform clouds in the Arctic and possible mechanisms for the production of high ice concentrations, Journal of Geophysical Research-Atmospheres, 106, 15065-15075, 10.1029/2000jd900286, 2001.

Richardson, M. S., DeMott, P. J., Kreidenweis, S. M., Cziczo, D. J., Dunlea, E. J., Jimenez, J. L., Thomson, D. S., Ashbaugh, L. L., Borys, R. D., Westphal, D. L., Casuccio, G. S., and Lersch, T. L.: Measurements of heterogeneous ice nuclei in the western United States in springtime and their relation to aerosol characteristics, Journal of Geophysical Research-Atmospheres, 112, 10.1029/2006jd007500, 2007.

Rinaldi, M., Fuzzi, S., Decesari, S., Marullo, S., Santoleri, R., Provenzale, A., von Hardenberg, J., Ceburnis, D., Vaishya, A., O'Dowd, C. D., and Facchini, M. C.: Is chlorophyll-a the best surrogate for organic matter enrichment in submicron primary marine aerosol?, Journal of Geophysical Research-Atmospheres, 118, 4964-4973, 10.1002/jgrd.50417, 2013.

Rinaldi, M., Santachiara, G., Nicosia, A., Piazza, M., Decesari, S., Gilardoni, S., Paglione, M., Cristofanelli, P., Marinoni, A., Bonasoni, P., and Belosi, F.: Atmospheric Ice Nucleating Particle measurements at the high mountain observatory Mt. Cimone (2165 m a.s.l., Italy), Atmospheric Environment, 171, 173-180, 10.1016/j.atmosenv.2017.10.027, 2017.

Rinaldi, M., Nicosia, A., Santachiara, G., Piazza, M., Paglione, M., Gilardoni, S., Sandrini, S., Cristofanelli, P., Marinoni, A., Bonasoni, P., Facchini, M. C., and Belosi, F.: Ground level ice nucleating particles measurements at Capo Granitola, a Mediterranean coastal site, Atmospheric Research, 219, 57-64, 10.1016/j.atmosres.2018.12.022, 2019.

Rogers, D. C., DeMott, P. J., Kreidenweis, S. M., and Chen, Y. L.: Measurements of ice nucleating aerosols during SUCCESS, Geophysical Research Letters, 25, 1383-1386, 10.1029/97gl03478, 1998.

Rolph, G., Stein, A., and Stunder, B.: Real-time Environmental Applications and Display sYstem: READY, Environmental Modelling & Software, 95, 210-228, 10.1016/j.envsoft.2017.06.025, 2017.

Santachiara, G., Di Matteo, L., Prodi, F., and Belosi, F.: Atmospheric particles acting as Ice Forming Nuclei in different size ranges, Atmospheric Research, 96, 266-272, 10.1016/j.atmosres.2009.08.004, 2010.

Santl-Temkiv, T., Lange, R., Beddows, D., Rauter, U., Pilgaard, S., Dall'Osto, M., Gunde-Cimerman, N., Massling, A., and Wex, H.: Biogenic Sources of Ice Nucleating Particles at the High Arctic Site Villum Research Station, Environmental Science & Technology, 53, 10580-10590, 10.1021/acs.est.9b00991, 2019.

Schiebel, T.: Ice nucleation activity of soil dust aerosols, Thesis, Karlsruhe Institute of Technology, 10.5445/IR/1000076327, 2017.

Schrod, J., Thomson, E. S., Weber, D., Kossmann, J., Pohlker, C., Saturno, J., Ditas, F., Artaxo, P., Clouard, V., Saurel, J. M., Ebert, M., Curtius, J., and Bingemer, H. G.: Long-term deposition and condensation ice-nucleating particle measurements from four stations across the globe, Atmospheric Chemistry and Physics, 20, 15983-16006, 10.5194/acp-20-15983-2020, 2020.

Schwikowski, M., Seibert, P., Baltensperger, U., and Gaggeler, H. W.: A STUDY OF AN OUTSTANDING SAHARAN DUST EVENT AT THE HIGH-ALPINE SITE JUNGFRAUJOCH, SWITZERLAND, Atmospheric Environment, 29, 1829-1842, 10.1016/1352-2310(95)00060-c, 1995.

Serreze, M. C. and Barry, R. G.: Processes and impacts of Arctic amplification: A research synthesis, Global and Planetary Change, 77, 85-96, 10.1016/j.gloplacha.2011.03.004, 2011.

Shaw, G. E.: The arctic haze phenomenon, Bulletin of the American Meteorological Society, 76, 2403-2413, 10.1175/1520-0477(1995)076<2403:tahp>2.0.co;2, 1995.

Shupe, M. D., Matrosov, S. Y., and Uttal, T.: Arctic mixed-phase cloud properties derived from surface-based sensors at SHEBA, Journal of the Atmospheric Sciences, 63, 697-711, 10.1175/jas3659.1, 2006.

Shupe, M. D., Walden, V. P., Eloranta, E., Uttal, T., Campbell, J. R., Starkweather, S. M., and Shiobara, M.: Clouds at Arctic Atmospheric Observatories. Part I: Occurrence and Macrophysical Properties, Journal of Applied Meteorology and Climatology, 50, 626-644, 10.1175/2010jamc2467.1, 2011.

Si, M., Irish, V. E., Mason, R. H., Vergara-Temprado, J., Hanna, S. J., Ladino, L. A., Yakobi-Hancock, J. D., Schiller, C. L., Wentzell, J. J. B., Abbatt, J. P. D., Carslaw, K. S., Murray, B. J., and Bertram, A. K.: Ice-nucleating ability of aerosol particles and possible sources at three coastal marine sites, Atmospheric Chemistry and Physics, 18, 15669-15685, 10.5194/acp-18-15669-2018, 2018.

Si, M., Evoy, E., Yun, J. W., Xi, Y., Hanna, S. J., Chivulescu, A., Rawlings, K., Veber, D., Platt, A., Kunkel, D., Hoor, P., Sharma, S., Leaitch, W. R., and Bertram, A. K.: Concentrations, composition, and sources of ice-nucleating particles in the Canadian High Arctic during spring 2016, Atmospheric Chemistry and Physics, 19, 3007-3024, 10.5194/acp-19-3007-2019, 2019.

Solomon, A., de Boer, G., Creamean, J. M., McComiskey, A., Shupe, M. D., Maahn, M., and Cox, C.: The relative impact of cloud condensation nuclei and ice nucleating particle concentrations on phase partitioning in Arctic mixed-phase stratocumulus clouds, Atmospheric Chemistry and Physics, 18, 17047-17059, 10.5194/acp-18-17047-2018, 2018.

Stein, A. F., Draxler, R. R., Rolph, G. D., Stunder, B. J. B., Cohen, M. D., and Ngan, F.: NOAA'S HYSPLIT ATMOSPHERIC TRANSPORT AND DISPERSION MODELING SYSTEM, Bulletin of the American Meteorological Society, 96, 2059-2077, 10.1175/bams-d-14-00110.1, 2015.

Stohl, A.: Characteristics of atmospheric transport into the Arctic troposphere, Journal of Geophysical Research-Atmospheres, 111, 10.1029/2005jd006888, 2006.

Tobo, Y.: An improved approach for measuring immersion freezing in large droplets over a wide temperature range, Scientific Reports, 6, 10.1038/srep32930, 2016.

Tobo, Y., Adachi, K., DeMott, P. J., Hill, T. C. J., Hamilton, D. S., Mahowald, N. M., Nagatsuka, N., Ohata, S., Uetake, J., Kondo, Y., and Koike, M.: Glacially sourced dust as a potentially significant source of ice nucleating particles, Nature Geoscience, 12, 253-+, 10.1038/s41561-019-0314-x, 2019.

Udisti, R., Bazzano, A., Becagli, S., Bolzacchini, E., Caiazzo, L., Cappelletti, D., Ferrero, L., Frosini, D., Giardi, F., Grotti, M., Lupi, A., Malandrino, M., Mazzola, M., Moroni, B., Severi, M., Traversi, R., Viola, A., and Vitale, V.: Sulfate source apportionment in the Ny-Alesund (Svalbard Islands) Arctic aerosol, Rendiconti Lincei-Scienze Fisiche E Naturali, 27, 85-94, 10.1007/s12210-016-0517-7, 2016.

Vali, G.: Quantitative evaluation of experimental results on the heterogeneous freezing nucleation of supercooled liquids, Journal of the Atmospheric Sciences, 28, 402-409, 1971.

Vali, G., DeMott, P. J., Mohler, O., and Whale, T. F.: Technical Note: A proposal for ice nucleation terminology, Atmospheric Chemistry and Physics, 15, 10263-10270, 10.5194/acp-15-10263-2015, 2015.

Vepuri, H. S. K., Rodriguez, C. A., Georgakopoulos, D. G., Hume, D., Webb, J., Mayer, G. D., and Hiranuma, N.: Ice-nucleating particles in precipitation samples from the Texas Panhandle, Atmospheric Chemistry and Physics, 21, 4503-4520, 10.5194/acp-21-4503-2021, 2021.

Wang, X. F., Sultana, C. M., Trueblood, J., Hill, T. C. J., Malfatti, F., Lee, C., Laskina, O., Moore, K. A., Beall, C. M., McCluskey, C. S., Cornwell, G. C., Zhou, Y. Y., Cox, J. L., Pendergraft, M. A., Santander, M. V., Bertram, T. H., Cappa, C. D., Azam, F., DeMott, P. J., Grassian, V. H., and Prather, K. A.: Microbial Control of Sea Spray Aerosol Composition: A Tale of Two Blooms, Acs Central Science, 1, 124-131, 10.1021/acscentsci.5b00148, 2015.

Wegener, A.: Thermodynamik der Atmosph¨are, Leipzig, Germany, 1911.

Welti, A., Bigg, E. K., DeMott, P. J., Gong, X. D., Hartmann, M., Harvey, M., Henning, S., Herenz, P., Hill, T. C. J., Hornblow, B., Leck, C., Loffler, M., McCluskey, C. S., Rauker, A. M., Schmale, J., Tatzelt, C., van Pinxteren, M., and Stratmann, F.: Ship-based measurements of ice nuclei concentrations over the Arctic, Atlantic, Pacific and Southern oceans, Atmospheric Chemistry and Physics, 20, 15191-15206, 10.5194/acp-20-15191-2020, 2020.

Westbrook, C. D. and Illingworth, A. J.: Evidence that ice forms primarily in supercooled liquid clouds at temperatures >-27 degrees C, Geophysical Research Letters, 38, 10.1029/2011gl048021, 2011.

Wex, H., DeMott, P. J., Tobo, Y., Hartmann, S., Rosch, M., Clauss, T., Tomsche, L., Niedermeier, D., and Stratmann, F.: Kaolinite particles as ice nuclei: learning from the use of different kaolinite samples and different coatings, Atmospheric Chemistry and Physics, 14, 5529-5546, 10.5194/acp-14-5529-2014, 2014.

Wex, H., Huang, L., Zhang, W., Hung, H., Traversi, R., Becagli, S., Sheesley, R. J., Moffett, C. E., Barrett, T. E., Bossi, R., Skov, H., Hunerbein, A., Lubitz, J., Loffler, M., Linke, O., Hartmann, M., Herenz, P., and Stratmann, F.: Annual variability of ice-nucleating particle concentrations at different Arctic locations, Atmospheric Chemistry and Physics, 19, 5293-5311, 10.5194/acp-19-5293-2019, 2019.

Wilson, T. W., Ladino, L. A., Alpert, P. A., Breckels, M. N., Brooks, I. M., Browse, J., Burrows, S. M., Carslaw, K. S., Huffman, J. A., Judd, C., Kilthau, W. P., Mason, R. H., McFiggans, G., Miller, L. A., Najera, J. J., Polishchuk, E., Rae, S., Schiller, C. L., Si, M., Temprado, J. V., Whale, T. F., Wong, J. P. S., Wurl, O., Yakobi-Hancock, J. D., Abbatt, J. P. D., Aller, J. Y., Bertram, A. K., Knopf, D. A., and Murray, B. J.: A marine biogenic source of atmospheric ice-nucleating particles, Nature, 525, 234-+, 10.1038/nature14986, 2015.

Wolf, M. J., Goodell, M., Dong, E., Dove, L. A., Zhang, C. Q., Franco, L. J., Shen, C. Y., Rutkowski, E. G., Narducci, D. N., Mullen, S., Babbin, A. R., and Cziczo, D. J.: A link between the ice nucleation activity and the biogeochemistry of seawater, Atmospheric Chemistry and Physics, 20, 15341-15356, 10.5194/acp-20-15341-2020, 2020.

915

Table 1. Compilation of previous ground level measurements of *n*INP in the Arctic

Reference	Location	Period	INP quantification method	Ice nucleation mode	*T* range (°C)	*n*INP (m^{-3})
Borys (1983)	Multiple	winter-summer	dynamic chamber	condensation	-16 to -28	<1-~80 (-16°C) ~50-~300 (-28°C)
Bigg (1996)	High Arctic (cruise)	1 August - 6 September 1991	static chamber	condensation	12.5, -15.0, -17.5	<1-250 (-15°C)
Bigg and Leck (2001)	High Arctic (cruise)	16 July - 23 September 1996	static chamber	condensation	-15	<1-~100
Conen et al. (2016)	Haldde observatory, Norway	02 - 06 July 2015	droplet freezing	immersion	-7 to -15	0-0.3 (-8°C) 1.7-12.2 (-15°C)
Mason et al. (2016)	Alert, Canada	29 March - 23 July 2014	droplet freezing	immersion	-15 to -25	50 (-15°C)* 220 (-20°C)* 990 (-25°C)*
Creamean et al. (2018)	Oliktok Point, Alaska	1 March - 31 May 2017	droplet freezing	immersion	-5 to -28	0.07-2 (10°C) 30-70 (-25°C)
Si et al. (2018)	Lancaster Sound, Canada	20 July 2014	droplet freezing	immersion	-15 to -25	0 (-15°C) 160 (-20°C) 670 (-25°C)
Irish et al. (2019)	Multiple (cruise)	14 July - 12 August 2014	droplet freezing	immersion	-15 to -25	5 (-15°C)* 44 (-20°C)* 154 (-25°C)*
Santl-Temkiv et al. (2019)	Villum, Greenland	summer 2016	droplet freezing	immersion	-6 to -20	17.8 (-10°C) 71.5 (-15 °C)
Si et al. (2019)	Alert, Canada	March 2016	droplet freezing	immersion	-10 to -30	5±2 (-15°C)* 20±4 (-20°C)* 186±40 (-25°C)*
Tobo et al. (2019)	Mt. Zeppelin, Svalbard	July 2016; March 2017	droplet freezing	immersion	-9 to -25	~1-5 (-15°C) 2-300 (-20°C) 30-~1000 (-25°C)
Wex et al. (2019)	Alert, Canada	May 2015 - April 2016	droplet freezing	immersion	-5 to -26	0.02-20 (-7°C) ~0.4-20 (-15°C) 10-20 (-23°C)
	Utqiagvik, Alaska	June 2012 - May 2013	droplet freezing	immersion	-5 to -26	0.02-20 (-7°C) 0.2-~20 (-15°C) ~3-~20 (-19°C)
	Ny-Ålesund, Svalbard	March - July 2012	droplet freezing	immersion	-5 to -26	<0.1-~0.7 (-7°C) 0.7-~30 (-15°C) ~30 (-23°C)
	Villum, Greenland	2015	droplet freezing	immersion	-5 to -26	<0.1-0.2 (-6°C) ~1-~10 (-15°C) ~20 (-20°C)
Welti et al. (2020)	High Arctic (cruise)	Multiple	droplet freezing	immersion	-5 to -40	1-20 (-15°C)
Schrod et al. (2020)	Mt. Zeppelin, Svalbard	May 2015 - Jan 2017	FRIDGE	condensation	-20 to -30	<40-~3000 (-20°C) <100-~2000 (-25°C)

* Average values

Table 2: Average (± standard deviation) and median (in brackets) *n*INP measured at GVB during 2018.

		-22°C			-18°C			-15°C		
		PM_1	PM_{10}	Coarse contrib.	PM_1	PM_{10}	Coarse contrib.	PM_1	PM_{10}	Coarse contrib.
		m^{-3}	m^{-3}	%	m^{-3}	m^{-3}	%	m^{-3}	m^{-3}	%
DFPC	Spring	97±48 (85)	116±42 (115)	21±22 (20)	45±25 (49)	55±28 (53)	20±20 (17)	13±9 (14)	18±9 (20)	32±36 (22)
	Summer	43±27 (38)	74±26 (77)	45±24 (48)	23±13 (23)	50±22 (47)	53±17 (58)	9±9 (7)	24±14 (20)	65±23 (72)
WT-CRAFT	Spring(*)	-	20±14 (19)	-	-	2±3 (1)	-	-	1±2 (-)	-
	Summer(**)		46±48 (37)	-	-	9±8 (6)	-	-	2±1 (2)	-

*16 April – 31 May 2018

**01 June - 15 August

925

Table 3a: Correlations of *n*INP, in PM_1 and PM_{10} samples by DFPC, with chemical tracers during the spring campaign. Coefficients reported in italic are statistically significant with p<0.10, while those in bold are statistically significant with p<0.05. Coefficients associated to p>0.2 have not been reported.

	-22°C		-18°C		-15°C	
	PM_1	PM_{10}	PM_1	PM_{10}	PM_1	PM_{10}
PM_{10} mass						*0.49*
Na^+	***-0.61***	*-0.49*	***-0.59***	-0.36	***-0.60***	
Mg^{+2}	***-0.52***		-0.38		-0.43	
Ca^{+2}		*0.45*			0.34	***0.64***
Cl^-	***-0.64***	*-0.51*	***-0.64***	-0.42	***-0.65***	
NO_3^-	***0.61***	***0.59***	***0.67***	***0.73***	***0.72***	***0.54***
MSA			-0.42	***-0.52***	-0.40	***-0.65***
Li^+	-0.36					
$nssSO_4^{-2}$	*0.43*	*0.44*	***0.53***	*0.43*	***0.62***	***0.67***
$nssK^+$	***0.60***	***0.56***	***0.68***	***0.56***	***0.77***	***0.72***

930 **Table 3b: Correlations of *n*INP, in PM_1 and PM_{10} samples by DFPC, with chemical tracers during the summer campaign. Coefficients reported in italic are statistically significant with p<0.10, while those in bold are statistically significant with p<0.05. Coefficients associated to p>0.2 have not been reported.**

	-22		-18		-15	
	PM_1	PM_{10}	PM_1	PM_{10}	PM_1	PM_{10}
PM_{10} mass				-0.35	-0.32	***-0.49***
Na^+		-0.36	-0.39	*-0.43*		***-0.52***
Mg^{+2}		-0.35	-0.41	*-0.48*	-0.35	***-0.57***
Ca^{+2}		-0.33	*-0.42*	*-0.44*		***-0.55***
Cl^-		-0.38	-0.37	*-0.45*		***-0.51***
NO_3^-					-0.33	-0.36
MSA						-0.37
Li^+		-0.32	-0.37	*-0.42*	-0.35	***-0.49***
$nssSO_4^{-2}$						-0.32
$nssK^+$	0.36					

Table 4a: Correlations of *n*INP by WT-CRAFT with chemical tracers during spring (April-May) 2018. Coefficients reported in italic are statistically significant with p<0.10, while those in bold are statistically significant with p<0.05. Coefficients associated to p>0.2 have not been reported.

	-15.0	-18.0	-20.0	-22.0	-24.0
PM_{10} mass	0.77	-0.63			
Na^{+}					
Mg^{+2}					
Ca^{+2}	*0.83*			*0.53*	0.47
Cl^{-}					
NO_3^{-}			***0.63***	***0.74***	*0.60*
MSA	*-0.81*			***-0.81***	***-0.82***
Li^{+}		-0.59			
$nssSO_4^{-2}$	0.75		0.43	***0.95***	***0.87***
$nssK^{+}$				***0.87***	***0.80***

Table 4b: Correlations of I *n*INP by WT-CRAFT with chemical tracers during summer (June-August) 2018. Coefficients reported in italic are statistically significant with p<0.10, while those in bold are statistically significant with p<0.05. Coefficients associated to p>0.2 have not been reported.

	-15.0	-18.0	-20.0	-22.0	-24.0
PM_{10} mass					
Na^{+}	*-0.45*	-0.36			-0.33
Mg^{+2}	-0.42	-0.37			
Ca^{+2}	-0.40				
Cl^{-}	-0.41	-0.38	-0.36		-0.37
NO_3^{-}		-0.38			
MSA					
Li^{+}					
$nssSO_4^{-2}$		*-0.44*			
$nssK^{+}$					

945 **Table 5: Correlation coefficient (R) resulting from the linear regression between *n*INP (at *T* = -15, -18 and -22°C) and the contribution of the four considered ground types. Values reported in bold are statistically significant (p<0.05).**

	DFPC_spring		
	INP_-15	INP-18	INP-22
Sea-Water	**-0.63**	**-0.54**	-0.39
Land	-0.05	0.36	-0.25
Sea-Ice	0.24	0.16	0.08
Snow	0.23	0.18	0.25
	DFPC_summer		
	INP_-15	INP-18	INP-22
Sea-Water	**-0.60**	-0.43	**-0.48**
Land	**0.86**	**0.72**	**0.65**
Sea-Ice	-0.15	-0.24	-0.11
Snow	0.39	0.32	0.33
	WT-CRAFT		
	INP_-15	INP-18	INP-22
Sea-Water	-0.04	0.17	0.02
Land	0.29	**0.54**	**0.42**
Sea-Ice	-0.21	-0.16	0.01
Snow	0.40	-0.19	-0.18

950

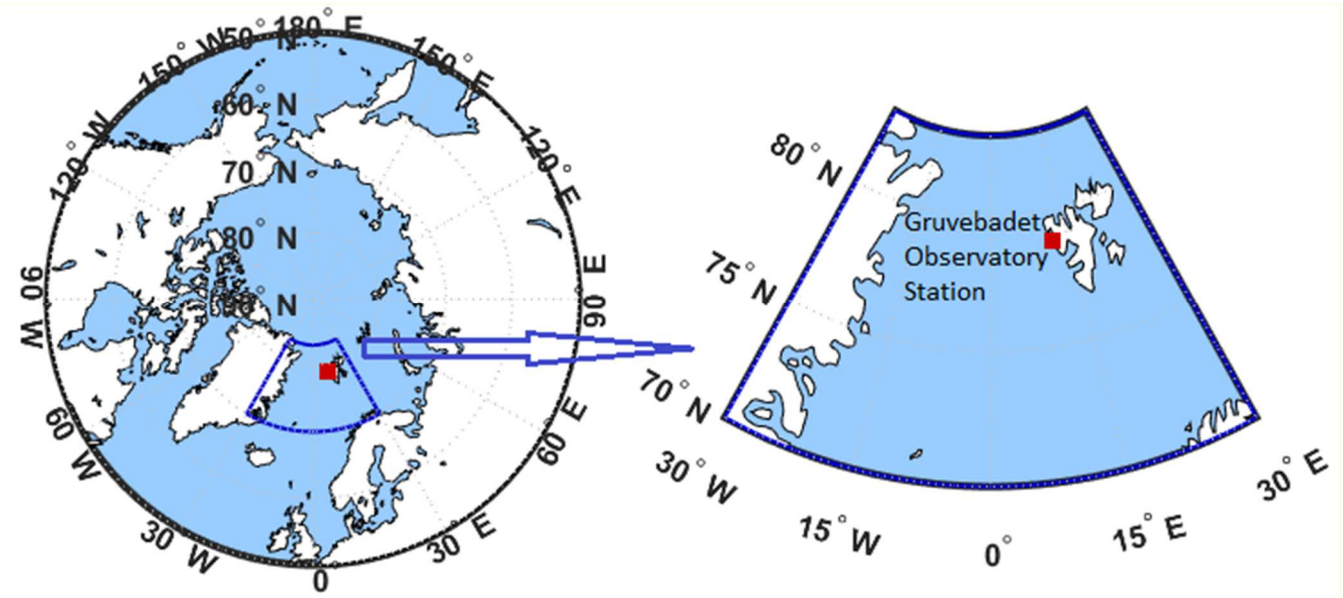

Figure 1: geographic location of the sampling station, Gruvebadet observatory at Ny-Ålesund, Svalbard Islands.

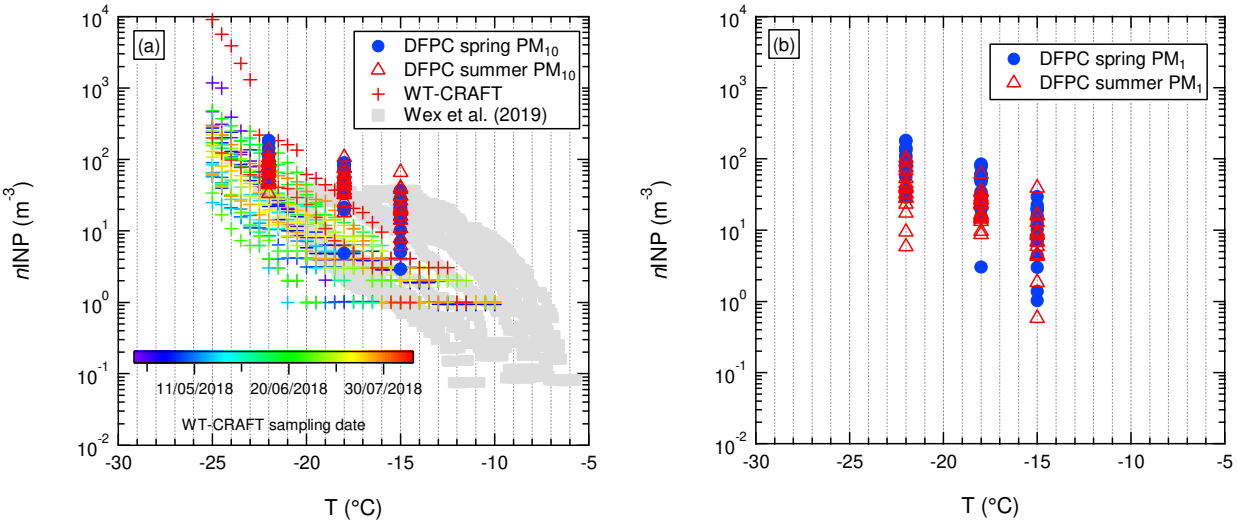

955 **Figure 2: Ambient *n*INP as a function of the activation *T* assessed for samples from GVB during 2018 by DFPC and WT-CRAFT. DFPC data are divided in spring (blue) and summer (red) samples, while WT-CRAFT data are color coded according to the sampling date. (a) PM_{10} (DFPC) and TSP (WT-CRAFT) data. (b) PM_1 data (available only for DFPC). For comparison purposes, the data from Wex et al. (2019), which refer to PM_{10} samples, are also reported in plot (a).**

960

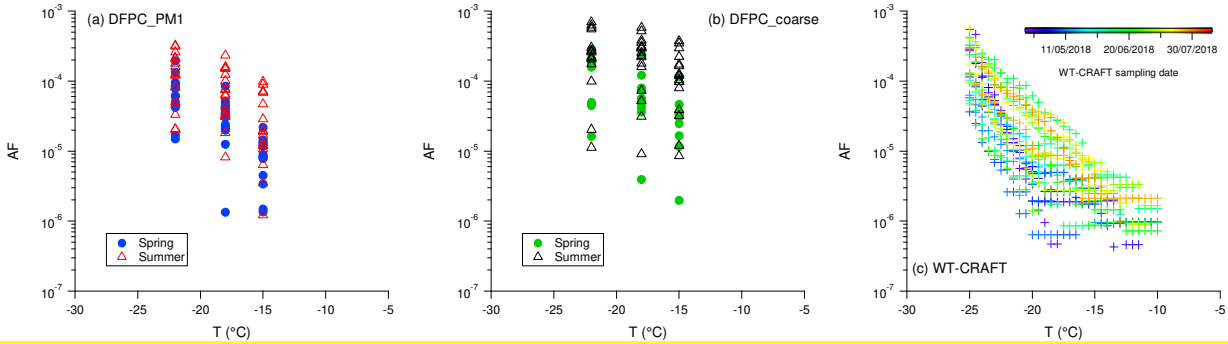

Figure 3: AF as a function of *T* assessed for samples from GVB during 2018 by DFPC in sub-micrometer (a) and coarse (b) size ranges and by WT-CRAFT (c).

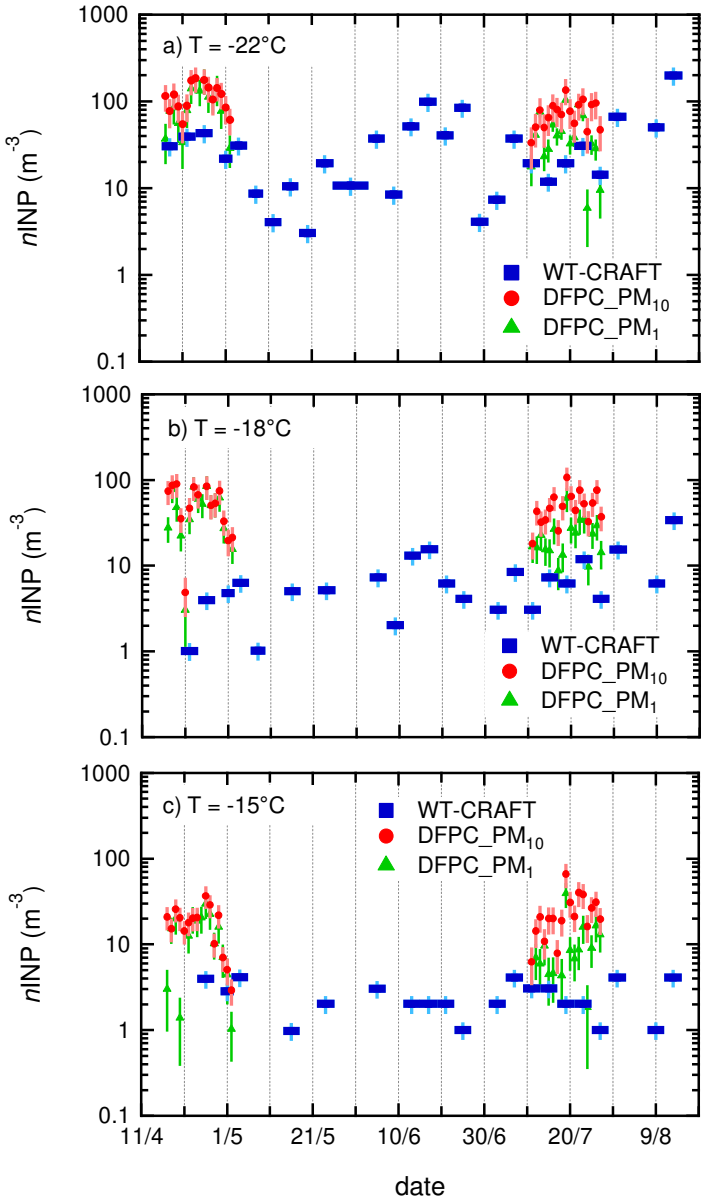

Figure 4: Time series of *n*INP at GVB during 2018 measured by DFPC (PM_{10} and PM_1) and WT-CRAFT. Horizontal bars indicate the time span of WT-CRAFT samples (ca. 4 days for the majority of samples). Vertical bars indicate the overall measurement uncertainty as indicated in the Sect. 2.

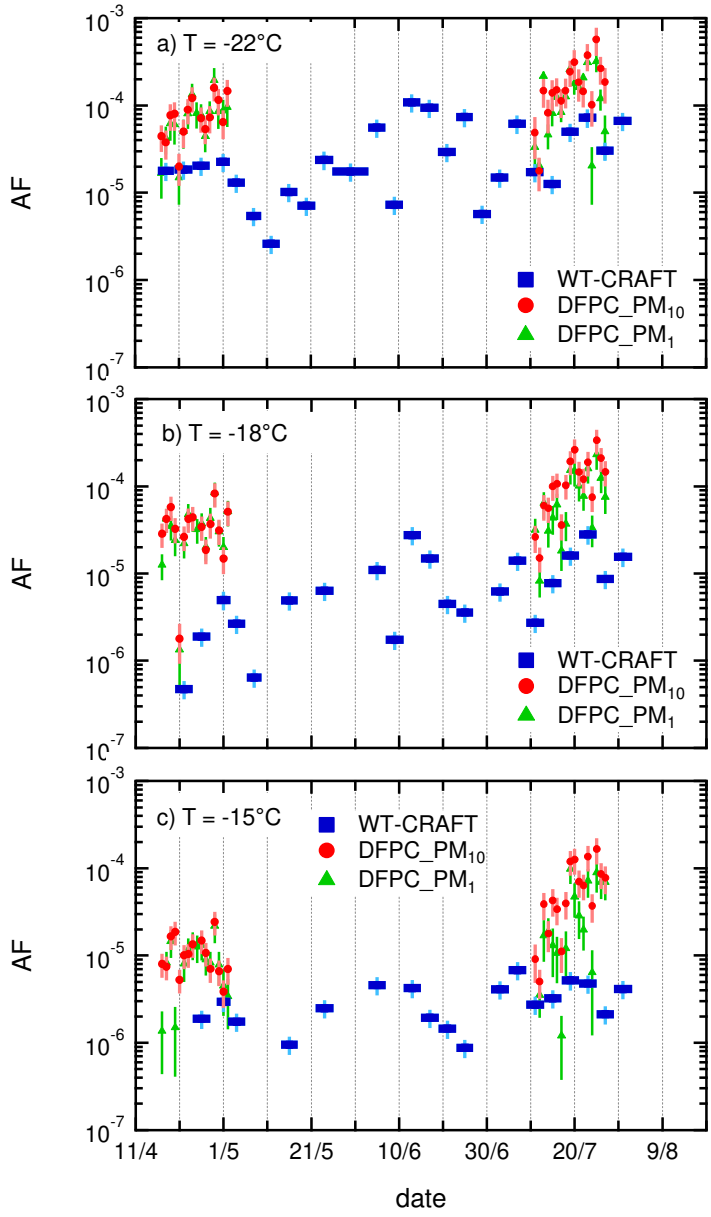

Figure 5: Time series of the activated fraction at GVB during 2018 measured by DFPC (PM_{10} and PM1) and WT-CRAFT. Horizontal bars indicate the time span of WT-CRAFT samples (ca. 4 days for the majority of samples). Vertical bars indicate the overall AF uncertainty, resultingh from the *n*INP uncertainty.

975

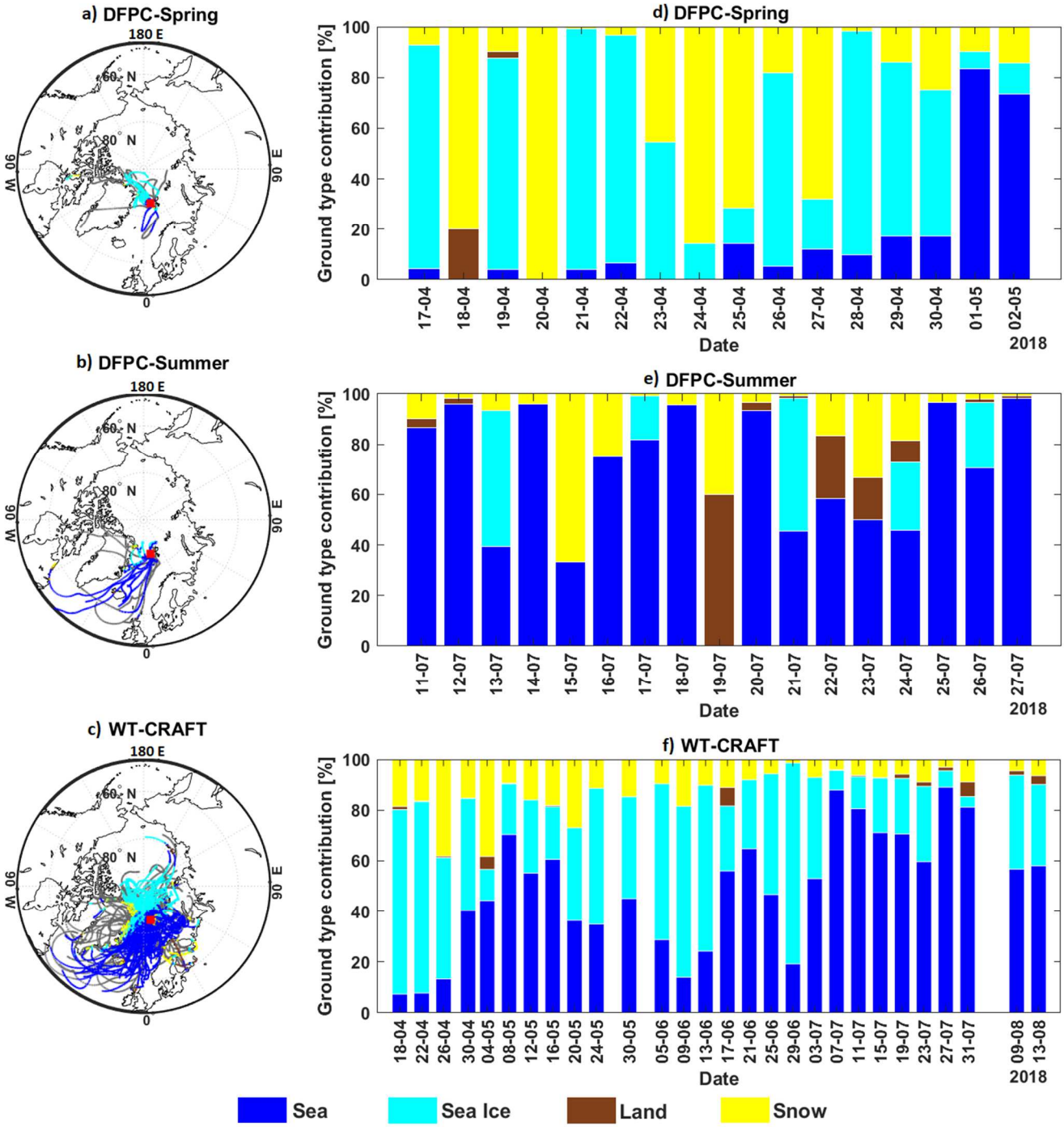

Figure 6: Air mass back-trajectories and ground type influence on low-travelling (<500 m) air masses for DFPC in spring (a), DFPC in summer (b) and WT-CRAFT (c) measurements. Back-trajectories reported in grey in the maps passed above 500 m amsl and were therefore excluded from the analysis. Ground type categories are described in Sect. 2.3.4.

980

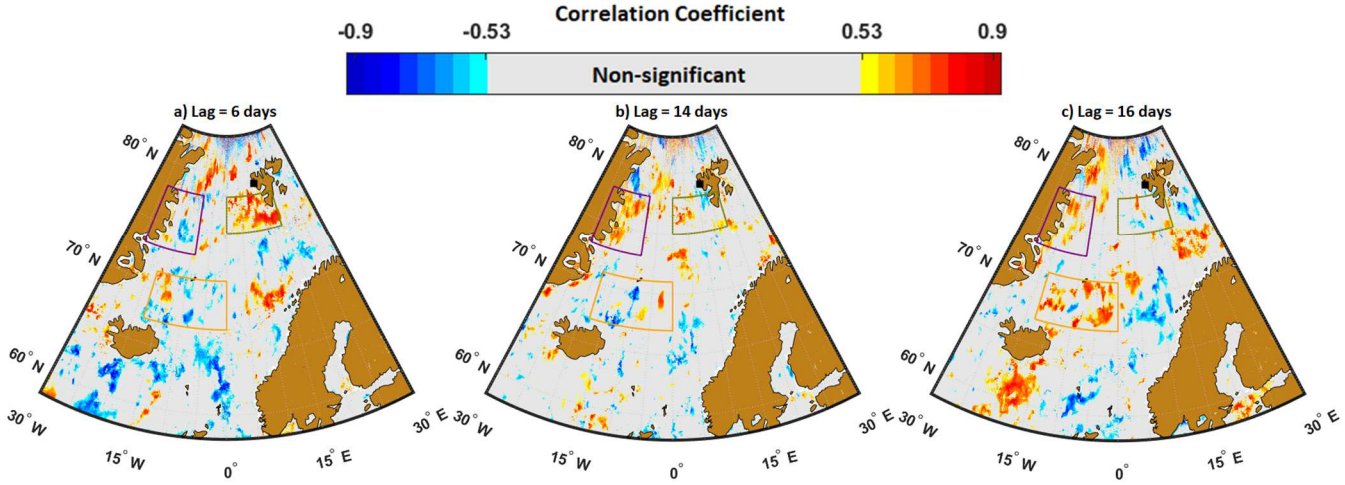

Figure 7: Correlation maps for nINP$_{PM1}$ at T = -15°C with (left) 6, (center) 14 and (right) 16 days time lag. The color scale indicates the correlation coefficient; not significant (p>0.05) pixels are reported in grey. The purple, green and orange boxes highlight sea regions characterized by high correlation at a certain time lag.

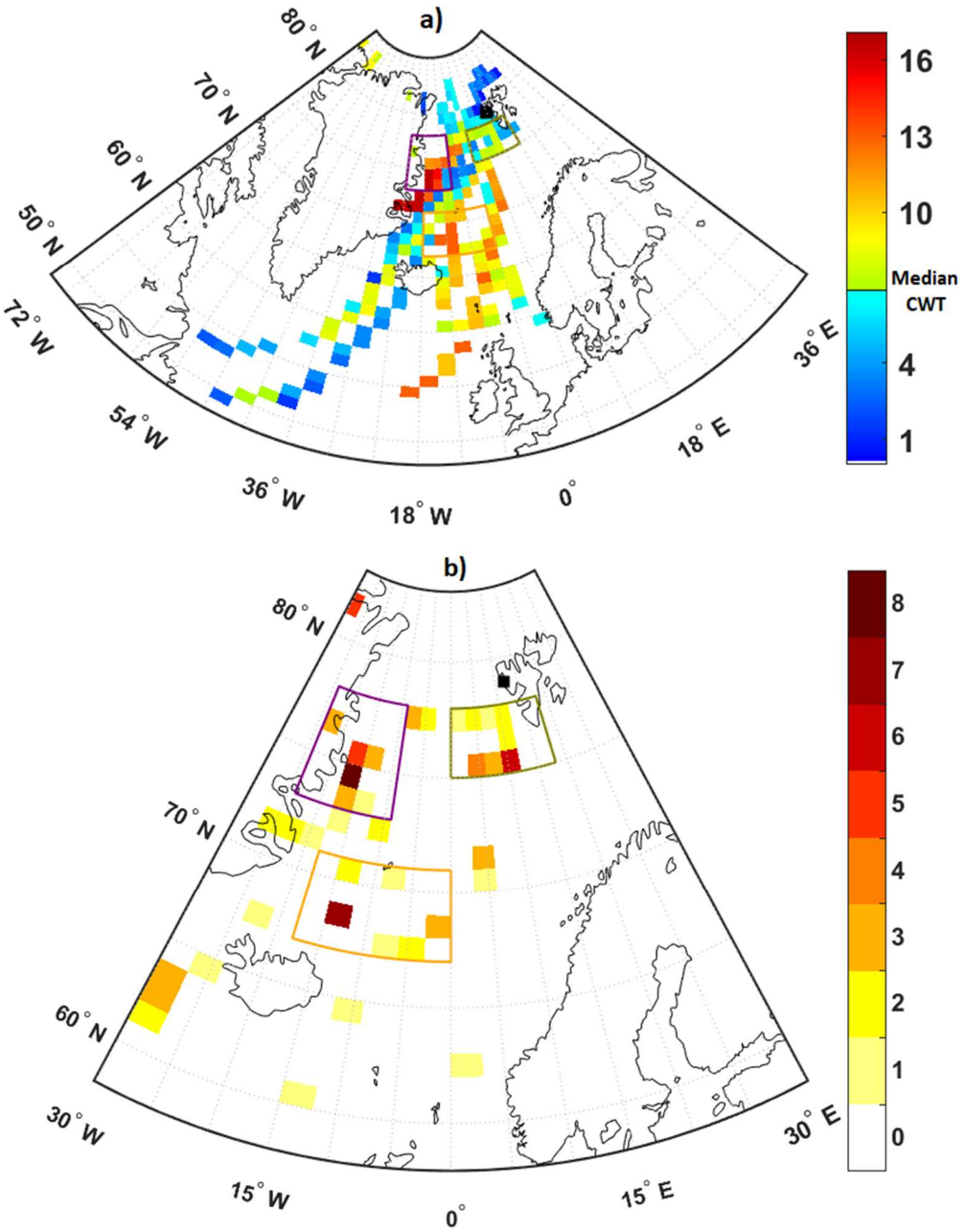

Figure 8. (a) CWT source map for the nINP$_{PM1}$ at T = -15°C dataset. The color scale indicate the CWT value. (b) Spatial distribution of fine INP sources identified by merging the results of the spatio-temporal correlation analysis and of the CWT algorithm. The color scale reflects how many times a given pixel has CWT ≥ median and significant correlation coefficient by running time lag from 5 to 20 days. The same purple, green and orange boxes of Figure 7 are reported to facilitate the comparison.